PROCEEDINGS A

royalsocietypublishing.org/journal/rspa

Research

Cite this article: Zhu C, Saintillan D, Chern A. 2025 Active nematic fluids on Riemannian two-manifolds. *Proc. R. Soc. A* **481**: 20240418. https://doi.org/10.1098/rspa.2024.0418

Received: 3 June 2024
Accepted: 13 February 2025

Subject Areas:
fluid mechanics, computational physics, mathematical physics

Keywords:
active nematics, surface Stokes flow, *k*-atic liquid crystal, Lie derivative, complex line, semi-Lagrangian

Author for correspondence:
David Saintillan
e-mail: dstn@ucsd.edu

Electronic supplementary material is available online at https://doi.org/10.6084/m9.figshare.c.7719737.

THE ROYAL SOCIETY PUBLISHING

Active nematic fluids on Riemannian two-manifolds

Cuncheng Zhu[1], David Saintillan[1] and Albert Chern[2]

[1]Department of Mechanical and Aerospace Engineering, and
[2]Department of Computer Science and Engineering,
University of California San Diego, La Jolla CA, USA

CZ, 0000-0003-1373-3492; DS, 0000-0001-9948-708X; AC, 0000-0002-9802-3619

Recent advances in cell biology and experimental techniques using reconstituted cell extracts have generated significant interest in understanding how geometry and topology influence active fluid dynamics. In this work, we present a comprehensive continuum theory and computational method to explore the dynamics of active nematic fluids on arbitrary surfaces without topological constraints. The fluid velocity and nematic order parameter are represented as the sections of the complex line bundle of a two-manifold. We introduce the Levi–Civita connection and surface curvature form within the framework of complex line bundles. By adopting this geometric approach, we introduce a gauge-invariant discretization method that preserves the continuous local-to-global theorems in differential geometry. We establish a nematic Laplacian on complex functions that can accommodate fractional topological charges through the covariant derivative on the complex nematic representation. We formulate advection of the nematic field based on a unifying definition of the Lie derivative, resulting in a stable geometric semi-Lagrangian (sL) discretization scheme for transport by the flow. In general, the proposed surface-based method offers an efficient and stable means to investigate the influence of local curvature and global topology on the two-dimensional hydrodynamics of active nematic systems.

1. Introduction

Active nematics, a unique class of systems defined by the interaction between intrinsic activity and orientational order, have emerged as a captivating paradigm to explore complex dynamical phenomena across scales. In biophysical contexts, deciphering the dynamics of these active matter systems offers profound insights into

a myriad of processes, encompassing collective dynamics in motile bacterial suspensions, structural organization in cytoskeletal assemblies, the dynamics of self-propelled colloidal particles and the processes governing tissue morphogenesis [1,2]. Recent experimental discoveries and the potential for significant advances in fields such as material science and biophysics have sparked a growing interest in understanding the intricate connections between the dynamic behaviour of active nematic systems and the geometric and topological constraints imposed by spatial confinement [3–13]. In this paper, we derive a minimal yet well-established model for active nematic systems on Riemannian surfaces from first principles using a geometric framework. This formulation allows us to develop a discrete theory and a corresponding numerical scheme that are efficient for general geometries. We expect the method to be a useful tool to study active nematic systems where the local curvature and global topology of the system are important, such as in morphogenesis, and to explore potential engineering applications in soft robotics and morphing materials.

To characterize nematic fields, the prevailing approach in the existing literature relies on the Landau–de Gennes $\boldsymbol{Q}$-tensor theory, which describes the configuration of the nematic field on a surface via a second-order symmetric tensor. However, in two dimensions, there exists an alternative representation through a homogeneous quadratic complex scalar function [14–16]. This approach offers distinct advantages because of the inherent constraints on its degrees of freedom. Unlike the complex representation, the evolution of the $\boldsymbol{Q}$-tensor needs to be confined within the realm of traceless and symmetric matrices, involving additional techniques such as Lagrange multipliers [17,18] or projection [19,20]. Furthermore, the complex representation facilitates a natural extension to k-atic fields (i.e. director fields with k-rotational symmetry) by simply raising the exponent of the complex function to k. Recently, there has been significant interest in modelling tissue dynamics through k-atic liquid crystal theory, highlighting the practical relevance of this approach [14,15].

The mathematical formulation of nematohydrodynamics, or more broadly of complex fluid flows, has been extensively explored in the literature [21–25]. Classic approaches primarily rely on an explicit approach, employing coordinate-based expressions and standard vector calculus. They often focus on the mechanics of specific physical objects in flow and root their arguments in the principle of material frame invariance [25]. These approaches become particularly challenging when attempting to translate ordinary vector calculus identities to curved surfaces. However, in the realm of differential geometry, there exists an abstract yet powerful geometric language, exemplified by the Lie derivative, which functions independently of coordinate systems. This language offers a natural way to comprehend various physical phenomena and conservation laws in fluid dynamics [26]. Concepts such as convected time derivatives in complex fluids can be effectively generalized through the use of the Lie derivative, unifying the derivation process. Despite its generality and utility, the adoption of this geometric language remains relatively obscure in applied fluid mechanics and is not widely recognized in the field of active nematics. In light of these challenges, our objective is to bridge this knowledge gap and recast a minimal active nematic system using the Lie derivative. This effort not only provides a unified perspective on the various components of the active nematohydrodynamic system but also, as we will demonstrate in the methods section, leads to a stable and elegant numerical approach [27–29].

Similar to the Lie derivative, we also seek to establish a coordinate-free framework for analysing active nematic fields on curved surfaces by using the mathematical structure called *fibre bundles*. This structure encapsulates the concept of a family of tensor spaces parameterized by a base manifold, providing a coordinate-free geometric language for describing tensor fields on the manifold as *sections* of bundles. When each *fibre* in the bundle is a one-dimensional complex vector space equipped with a Riemannian metric, which houses the k-atic director and velocity vector, this bundle is considered a Hermitian complex line bundle. The theory of the complex line bundle has been the subject of extensive research in both pure mathematics and theoretical physics, particularly in modelling condensed matter phenomena [30]. The Levi–Civita connection on the tangent bundle induces an associated connection on to the nematic bundle, which gives rise to a nematic Bochner Laplacian that accommodates fractional topological defects

under the relaxation of nematic elasticity. The nuanced difference between the nematic and vector Bochner Laplacians has often been overlooked or inadequately explored in the existing literature. In addition to the theoretical advancement it provides, this complex line representation also facilitates the construction of an intrinsic complex-valued discrete Laplacian matrix based on the local chart, instead of relying on a global parametrization or an $\mathbb{R}^3$ representation in the embedded coordinate. Overall, the formalism grounded in the complex line bundle theory unveils a richer perspective on the representation of nematic—and more broadly *k*-atic—fields, across arbitrary two-dimensional manifolds.

We also show how one can formulate the Stokes equations through the Dolbeault operators in the complex line bundle theory. On a Riemannian manifold, the measurement of strain rate is determined by the symmetric part of the covariant derivative, commonly referred to as the Killing operator. With the complex structure, the covariant derivative can be orthogonally decomposed into the holomorphic *Del* and the anti-holomorphic *Del bar* operators, jointly known as the Dolbeault operators. We elucidate that, under the incompressibility condition, the Laplacian-like operator that determines the viscous stress on a Riemannian manifold is induced by the Del bar operator. In addition to the Bochner Laplacian, this operator encompasses contributions from the curvature of the manifold. This fact is acknowledged in the literature, despite the results having been derived from the perspective of Riemannian geometry [26,31,32]. While both derivations are equivalent in this specific case, we believe that the more general formulation based on complex line bundles can reveal new perspectives and potential for further theoretical or computational advancements.

In the computational realm, several efforts have previously been undertaken to solve active fluid dynamics on curved surfaces. These endeavours are founded on continuum formulations [33–36] or on the Lattice Boltzmann method [10,37]. In particular, we highlight the limitations of using the streamfunction formulation for incompressible fluid mechanics on manifolds with non-trivial topology without specialized modifications [35,38–42]. However, one common challenge with velocity–pressure-based methods is the representation of tangent vectors. In our method, we represent both the velocity and director using an intrinsic complex-valued function alongside the Levi–Civita connection. This approach eliminates the need for the commonly used numerical technique of constraining the $\mathbb{R}^3$-valued velocity to lie tangent to the manifold [35,43]. Moreover, we draw parallels between the numerical scheme for active nematics and classic problems in computational geometry. For example, insightful analogies can be found from the resemblance between the Stokes equations and the computation of Killing vector fields, which aid in discerning symmetries within geometries [44–47]. Similarly, there is a correspondence between the modelling of *k*-atic liquid crystals with vector field design, which has been developed in applications such as mesh and texture generation [47–49].

The rest of the paper is structured as follows. We first introduce the geometric formulation of active nematics in a continuous setting in §2. This is followed by the development of a discretization approach that adheres to the underlying geometric principles in §3. Results are discussed in §4, where we present numerical solutions for the dynamics of active nematics on diverse geometries, highlighting the ability of our framework to capture the intricate dynamics under various flow regimes and surface topologies. We conclude and discuss potential extensions of this work in §5.

2. Theoretical formulation

An active fluid is a type of fluid for which the constituent elements have the ability to exert internal mechanical stresses. In biological systems composed of microscopic particles, inertia is negligible due to the small size and low velocities, resulting in low-Reynolds-number flow (i.e. Stokes flow). Here, the fluid flow is driven by the active stresses induced by the constituent elements. In active nematics, microscopic constituents with orientation $\boldsymbol{q}$ exhibit nematic symmetry, meaning there is an equivalence relation between orientations $\boldsymbol{q}$ and $-\boldsymbol{q}$. The configuration of the nematic field is governed by the nematodynamics equation, an

advection–diffusion equation acting on this orientation. Because the system operates on a curved Riemannian surface and our discretization method is devoid of global coordinates, we first introduce the system of equations through an abstract geometric language and then present the explicit expression in a later section.

(a) Mathematical framework

In this section, we will establish the geometric framework required to formulate the hydrodynamics of active nematics on a two-dimensional Riemannian manifold. In §§2a(i) and (ii), we introduce the complex representation of a k-atic director, specifically for the tangent vector and the nematic director. In §2a(iii), we introduce the Lie derivative on tensor fields, which is crucial for describing transport phenomena and deformations in fluid mechanics. The Bochner Laplacian governs the relaxation dynamics of vector and nematic fields. We start by introducing the Levi–Civita connection (i.e. covariant derivative) on the tangent bundle in §2a(iv), which enables us to extend the discussion to the nematic connection in §2a(v) and the Bochner Laplacian on each bundle in §2a(vi). In §2a(vii), we detect and quantify charges associated with nematic topological defects by measuring the total rotation of a director field along a closed loop using the Levi–Civita connection.

(i) Order parameter of k-atic director

We first introduce the general description for a k-atic director in the plane, such as a vector ($k=1$) and a nematic director ($k=2$). Let V be a two-dimensional Euclidean vector space, and the multiplicative group action of complex numbers, $\mathbb{C}^\times$, on V is given by

$$\mathbb{C}^\times \times V \to V, \quad (re^{\mathbf{i}\theta}, \boldsymbol{u}) \mapsto \mathrm{Scale}(\mathrm{Rotate}(\boldsymbol{u}, \theta), r). \tag{2.1}$$

A finite subgroup of rotation actions, $N = \{1, e^{\mathbf{i}2\pi/k}, \ldots, e^{\mathbf{i}(k-1)2\pi/k}\} \subset \mathbb{C}^\times$, defines an equivalence relation of k-rotational symmetry denoted by $\sim$. For any $\boldsymbol{u}, \boldsymbol{v} \in V$, we have

$$\boldsymbol{u} \sim \boldsymbol{v} \quad \text{iff} \quad \exists \quad \hat{z} \in N \quad \text{s.t. } \boldsymbol{v} = \hat{z}\boldsymbol{u}. \tag{2.2}$$

This equivalence relation allows us to define a quotient set $V_k = V/N$ and the map of taking the equivalence class $[\cdot]_k : V \to V_k$. Each element $[\boldsymbol{q}]_k \in V_k$ is called a k-atic director. The action of $\mathbb{C}^\times$ on V naturally induces a canonical quotient action $\mathbb{C}_k^\times = \mathbb{C}^\times/N$ on V_k, given by

$$\mathbb{C}_k \times V_k \to V_k, \quad (r^k e^{\mathbf{i}k\theta}, [\boldsymbol{u}]_k) \mapsto [re^{i\theta}\boldsymbol{u}]_k, \tag{2.3}$$

where the rotational group is partitioned in θ, with $e^{\mathbf{i}k\theta} \sim \hat{z}e^{\mathbf{i}k\theta}, \hat{z} \in N$. Formally, we have the power map $P : \mathbb{C}^\times \to \mathbb{C}^\times$, $re^{\mathbf{i}\theta} \mapsto r^k e^{\mathbf{i}k\theta}$, which is a homomorphism with kernel being exactly N. By the first isomorphism theorem [50], $\mathbb{C}^\times/\ker(P) \cong \mathrm{im}(P)$, the quotient group is isomorphic to the image of the map, $\mathbb{C}_k^\times \cong \mathrm{im}(P) = \mathbb{C}^\times$. If, given a unit basis vector $\mathbf{1} \in V$ with $|\mathbf{1}| = 1$, we can establish an isomorphism between complex numbers $\mathbb{C} \ni \hat{q}$ and vectors $V \ni \boldsymbol{q}$ by $\boldsymbol{q} = \hat{q}\mathbf{1} = re^{\mathbf{i}\theta}\mathbf{1} \in V$. Similarly, given a k-director basis $[\mathbf{1}]_k \in V_k$, we can establish the isomorphism between $\mathbb{C} \ni [\hat{q}]_k$ and its associated k-director $V_k \ni [\boldsymbol{q}]_k = [\hat{q}]_k[\mathbf{1}]_k = r^k e^{\mathbf{i}k\theta}[\mathbf{1}]_k = \hat{q}^k[\mathbf{1}]_k$. Through the chain rule, the *pushforward* of the equivalence map, denoted as $d[]_k|_{\boldsymbol{q}}$, maps an increment vector, $\boldsymbol{q}' \in T_{\boldsymbol{q}}V$, to an increment k-atic director, $[\boldsymbol{q}]_k' = k[\boldsymbol{q}]_{k-1}\boldsymbol{q}' \in T_{[\boldsymbol{q}]_k}V_k$.

When focusing on a nematic field with $k=2$ and $N=\{1,-1\}$, an alternative representation of the equivalence class is through a rank-1 symmetric tensor $[\boldsymbol{q}]_2 \cong \boldsymbol{q} \otimes \boldsymbol{q} \in \mathcal{Q}$, where $\mathcal{Q} = \{\, \boldsymbol{Q} \in V \otimes_{\mathrm{symm}} V \mid \mathrm{rank}\, \boldsymbol{Q} \le 1 \,\}$. We called the bijective map from the representation of complex numbers to the matrix representation the *Veronese map*,

$$\mathcal{V} : V_2 \to \mathcal{Q}, \quad [\boldsymbol{q}]_2 \mapsto \boldsymbol{q} \otimes \boldsymbol{q}. \tag{2.4}$$

For clarity, in the reminder of this paper, we will omit the subscript and specify the bracket to denote a nematic equivalence (i.e. $[] = []_2$). With $[\boldsymbol{q}] \in V_2$, $\boldsymbol{Q} = \mathcal{V}([\boldsymbol{q}]) \in \mathcal{Q}$, the pushforward of the Veronese map $d\mathcal{V} : T_{[\boldsymbol{q}]}V_2 \to T_{\boldsymbol{Q}}\mathcal{Q}$ maps an increment $[\boldsymbol{q}]'$ in complex representation to the increment in matrix representation $\boldsymbol{Q}'$.

(ii) Vector field and nematic field on a Riemannian manifold

On a closed Riemannian two-manifold M, $\partial M = \varnothing$, each point $p \in M$ has a tangent space T_pM that is a copy of the Euclidean plane: $T_pM \cong V$. Tangent spaces at different points, T_pM, T_qM, for $p \neq q$, are disjoint spaces (spaces with no elements in common), and the disjoint union (a union where elements are kept separate rather than merged) of all tangent spaces is referred to as the *tangent bundle*, $TM = \bigcup_p T_pM$. Here, the tangent space T_pM is also referred to as the *fibre* of the *fibre bundle* TM at a base point $p \in M$. A tangent vector field $\boldsymbol{q}$ is described as a *section* of the tangent bundle, $\boldsymbol{q} \in \Gamma(TM)$, which is an assignment of a fibre element $\boldsymbol{q}_p \in T_pM$ at each point $p \in M$. We also denote a section defined over a region $U \subset M$ as $\boldsymbol{q} \in \Gamma_U(TM)$.

Similarly, we can describe a nematic field as a section of the nematic bundle L, $[\boldsymbol{q}] \in \Gamma(L)$. Each fibre of the nematic bundle L at $p \in M$, L_p, is given by the equivalence relation, $L_p := [T_pM]$ $(= [T_pM]_2)$ (cf. §2a(i)). In other words, the nematic bundle $L = [TM]$ is obtained by taking the fibre-wise equivalence class of the tangent bundle.

With a basis section for the tangent bundle, $\mathbf{1} \in \Gamma_U(TM)$, $|\mathbf{1}| = 1$, defined in a neighbourhood $U \subset M$, we can construct the corresponding nematic basis section for L as $[\mathbf{1}] \in \Gamma_U(L)$. Basis sections allow us to represent vector fields and nematic fields by complex scalar functions, $\hat{q} : U \to \mathbb{C}$ and $[\hat{q}] : U \to \mathbb{C}_2$.

Recall that a nematic vector $[\boldsymbol{q}]$ can also be represented by a rank-1 symmetric tensor via the Veronese map of equation (2.4). We can similarly represent a nematic field as a section of the symmetric rank-1 tensor bundle as follows. The complex representation of the nematic field is isomorphic to a tensor field $\boldsymbol{Q} = \boldsymbol{q} \otimes \boldsymbol{q} \in \Gamma(E)$, where E is the fibre bundle given by the set $\mathcal{Q}$ of rank ≤ 1 in the symmetric tensor bundle $TM \otimes_{\text{symm}} TM$. By populating the fibre-wise Veronese map $\mathcal{V} : V_2 \to \mathcal{Q}$, we get the section-wise map $\mathcal{V} : \Gamma(L) \to \Gamma(E)$.

The Riemannian metric structure, $\boldsymbol{g}|_p : T_pM \times_{\text{symm}} T_pM \to \mathbb{R}$, provides a positive-definite inner product $\langle \cdot, \cdot \rangle = \boldsymbol{g}(\cdot, \cdot)$ between tangent vector fields or nematic fields. For any two vector fields $\boldsymbol{u} = \hat{u}\mathbf{1}$, $\boldsymbol{v} = \hat{v}\mathbf{1}$ and two nematic fields $[\boldsymbol{q}] = [\hat{q}][\mathbf{1}] \cong \boldsymbol{q} \otimes \boldsymbol{q}$, $[\boldsymbol{p}] = [\hat{p}][\mathbf{1}] \cong \boldsymbol{p} \otimes \boldsymbol{p}$, the inner products are defined using their complex representations,

$$\langle \cdot, \cdot \rangle : \begin{cases} V \times V \to \mathbb{R}, & \langle \boldsymbol{u}, \boldsymbol{v} \rangle \mapsto \Re(\hat{u}\bar{\hat{v}}), \\ V_2 \times V_2 \to \mathbb{R}, & \langle [\boldsymbol{q}], [\boldsymbol{p}] \rangle \mapsto \Re([\hat{q}][\overline{\hat{p}}]), \\ \mathcal{Q} \times \mathcal{Q} \to \mathbb{R}, & \langle \boldsymbol{p} \otimes \boldsymbol{p}, \boldsymbol{q} \otimes \boldsymbol{q} \rangle = \langle \boldsymbol{p}, \boldsymbol{q} \rangle^2 \mapsto (\Re(\hat{q}\bar{\hat{p}}))^2, \end{cases} \tag{2.5}$$

where $\bar{\cdot}$ denotes complex conjugation. Note that the inner product for $\mathcal{Q}$ is the Frobenius inner product that can be extended and denoted as $\boldsymbol{G} = \boldsymbol{g} \otimes \boldsymbol{g} : (V \otimes V) \times (V \otimes V) \to \mathbb{R}$. A functional that maps a tangent vector field to a scalar function, $\alpha : T_pM \to \mathbb{R}$, is referred to as a *covector* field. A natural *dual pairing* of α with a vector field $\boldsymbol{u}$ is denoted as $\alpha[\![\boldsymbol{u}]\!]$. We denote this as $\alpha \in \Gamma(T^*M)$, where T^*M is known as the cotangent bundle, which is the dual space to the tangent bundle. The metric provides a way to associate a vector with its dual counterpart, $\boldsymbol{g}|_p : T_pM \to T_p^*M$, where a vector $\boldsymbol{u}$ is mapped to $\boldsymbol{g}(\boldsymbol{u}, \cdot)$. In index notation, this is referred to as *lowering* an index, and it can be expressed as $u_i = g_{ij}u^j$. Similarly, the Frobenius inner product $\boldsymbol{G}|_p : (T_pM \otimes T_pM) \to (T_p^*M \otimes T_p^*M)$ provides a way to map a $(2,0)$ tensor to a $(0,2)$ tensor, or $P_{ij} = g_{im}g_{jn}P^{mn}$ in index notation. With the metric, we can define the L_2 inner product of a vector or nematic field on M as $\langle\!\langle \cdot, \cdot \rangle\!\rangle := \int_M \langle \cdot, \cdot \rangle \, \mathrm{d}A : \Gamma(\circ) \times \Gamma(\circ) \to \mathbb{R}$. The corresponding metric norm and L_2 norm are denoted as $|\cdot|$ and $||\cdot||$, respectively.

(iii) Flow, Lie derivative and advection

On a manifold, the Lie derivative provides a generalized framework for assessing changes in tensor fields encompassing functions with scalar, vector and covector values, along the flow defined by another vector field [51–53].

Consider an instantaneous flowmap $\varphi(t) : M \to M$ generated by a velocity field $\boldsymbol{u} \in \Gamma(TM)$ such that $\dot{\varphi} = \boldsymbol{u}$, $\varphi(0) = \mathrm{id}_M$. The flowmap φ induces a pushforward map on the tangent space, $\mathrm{d}\varphi|_p : T_pM \to T_{\varphi(p)}M$. In continuum mechanics, the pushforward map is known as the deformation

gradient $\boldsymbol{F}$ and satisfies $\mathrm{d}\varphi|_p(\boldsymbol{q}) = \boldsymbol{F}\boldsymbol{q}$. We can deduce from linearity that $\mathrm{d}\varphi([\boldsymbol{q}]) = [\mathrm{d}\varphi(\boldsymbol{q})] = [\boldsymbol{F}\boldsymbol{q}]$. This is equivalent to the map on the matrix representation $\boldsymbol{Q}$, $\mathrm{d}\varphi(\boldsymbol{q}\otimes\boldsymbol{q}) = \mathrm{d}\varphi(\boldsymbol{q})\otimes\mathrm{d}\varphi(\boldsymbol{q}) = \boldsymbol{F}\boldsymbol{Q}\boldsymbol{F}^\top$. To summarize, we have the pushforward map defined as

$$\mathrm{d}\varphi : \begin{cases} \Gamma(TM)\to\Gamma(TM), & \mathrm{d}\varphi(\boldsymbol{q}) = \boldsymbol{F}\boldsymbol{q}, \\ \Gamma(L)\to\Gamma(L), & \mathrm{d}\varphi([\boldsymbol{q}]) = [\boldsymbol{F}\boldsymbol{q}], \\ \Gamma(E)\to\Gamma(E), & \mathrm{d}\varphi(\boldsymbol{Q}) = \boldsymbol{F}\boldsymbol{Q}\boldsymbol{F}^\top. \end{cases} \tag{2.6}$$

For a covector field $\boldsymbol{\alpha}\in\Gamma(T^*M)$, the pullback map $\varphi^* : T^*_{\varphi(p)}M \to T^*_pM, \varphi^*\boldsymbol{\alpha}\mapsto(\mathrm{d}\varphi)^\top\boldsymbol{\alpha} = \boldsymbol{F}^\top\boldsymbol{\alpha}$, is the adjoint of the pushforward map. Because the metric $\boldsymbol{g}\in\Gamma(T^*M\otimes_{\mathrm{symm}}T^*M)$ is a valence $(0,2)$ tensor, its pullback map follows $\varphi^*\boldsymbol{g}\mapsto\boldsymbol{F}^\top\boldsymbol{g}\boldsymbol{F}$. Since the pullback map preserves the dual pairing, $\varphi^*(\alpha[\![\boldsymbol{q}]\!]) = \varphi^*\alpha[\![\varphi^*\boldsymbol{q}]\!]$, a pullback map for a vector field is the inverse map of the pushforward $\varphi^*|_p = (\mathrm{d}\varphi|_p)^{-1} = \boldsymbol{F}^{-1} : T_{\varphi(p)}M\to T_pM$. With omission of the precomposition for non-scalar fields (e.g. $\boldsymbol{q}\circ\varphi$ is denoted as $\boldsymbol{q}$), we can summarize pullback maps as

$$\varphi^* : \begin{cases} C^\infty(M)\to C^\infty(M), & \varphi^*f = f\circ\varphi, \\ \Gamma(G)\to\Gamma(G), & \varphi^*\boldsymbol{g} = \boldsymbol{F}^\top\boldsymbol{g}\boldsymbol{F}, \\ \Gamma(TM)\to\Gamma(TM), & \varphi^*\boldsymbol{q} = \boldsymbol{F}^{-1}\boldsymbol{q}, \\ \Gamma(L)\to\Gamma(L), & \varphi^*[\boldsymbol{q}] = [\boldsymbol{F}^{-1}\boldsymbol{q}], \\ \Gamma(E)\to\Gamma(E), & \varphi^*\boldsymbol{Q} = \boldsymbol{F}^{-1}\boldsymbol{Q}\boldsymbol{F}^{-\top}. \end{cases} \tag{2.7}$$

The Lie derivative is defined as the rate of change of the time-varying pullback field at $t=0$,

$$\left.\frac{\partial}{\partial t}\right|_{t=0}\circ\varphi^* =: \frac{\partial}{\partial t} + \mathcal{L}_{\dot\varphi} : \begin{cases} \dot f + \mathcal{L}_{\boldsymbol{u}}f & = \lim_{t\to0}(f_{\varphi(p)} - f_p)/t, \\ \mathcal{L}_{\boldsymbol{u}}\boldsymbol{g} & = \lim_{t\to0}(\boldsymbol{F}^\top\boldsymbol{g}_{\varphi(p)}\boldsymbol{F} - \boldsymbol{g}_p)/t, \\ \dot{\boldsymbol{q}} + \mathcal{L}_{\boldsymbol{u}}\boldsymbol{q} & = \lim_{t\to0}(\boldsymbol{F}^{-1}\boldsymbol{q}_{\varphi(p)} - \boldsymbol{q}_p)/t, \\ [\dot{\boldsymbol{q}}] + \mathcal{L}_{\boldsymbol{u}}[\boldsymbol{q}] & = \lim_{t\to0}([\boldsymbol{F}^{-1}\boldsymbol{q}_{\varphi(p)}] - [\boldsymbol{q}]_p)/t, \\ \dot{\boldsymbol{Q}} + \mathcal{L}_{\boldsymbol{u}}\boldsymbol{Q} & = \lim_{t\to0}(\boldsymbol{F}^{-1}\boldsymbol{Q}_{\varphi(p)}\boldsymbol{F}^{-\top} - \boldsymbol{Q}_p)/t. \end{cases} \tag{2.8}$$

Here, we assume that the metric is time-independent, $\dot{\boldsymbol{g}} = 0$. In continuum mechanics, the Lie derivative of scalar function recovers the familiar material derivative. When applied to a vector and nematic field, the Lie derivative is the upper-convected derivative [54]. The Lie derivative of the metric, $\mathcal{L}_{\boldsymbol{u}}\boldsymbol{g}$, is the strain rate tensor that measures the rate of change of the Green–Lagrange strain tensor, $\boldsymbol{F}^\top\boldsymbol{g}\boldsymbol{F} - \boldsymbol{g}$. A section $\boldsymbol{\psi}$ is said to be *Lie advected* by the flow φ when $\partial\varphi^*\boldsymbol{\psi}/\partial t = 0$.

In summary, the Lie derivative generalizes the concept of advection from scalar functions to tensor fields. This theoretical framework is not only mathematically satisfying but also practical, as it enables the development of a unifying geometric discretization (cf. §3b) that forgoes the use of coordinate-based expressions and respects the underlying continuous structure.

(iv) Levi–Civita connection on the tangent bundle

On a curved space, each tangent space is in general different from other tangent spaces. The Levi–Civita connection introduces the concept of parallel transport, allowing us to compare vectors at different points along a curved manifold. Given a parametrized segment on M, $\gamma(t) : [-\epsilon,\epsilon]\to M$, with the starting point $\gamma(0) = p$ and velocity $\gamma'(0) = \boldsymbol{v}$, parallel transport is a one-parameter family of linear maps dependent on the path γ, denoted as $\Pi_{p\rightsquigarrow\gamma(t)} : T_pM\to T_{\gamma(t)}M$, with $t\in[-\epsilon,\epsilon]$ [55]. Parallel transport allows us to express the directional covariant derivative of $\boldsymbol{u}\in\Gamma(TM)$ with respect to $\boldsymbol{v}$ as follows:

$$\nabla_{\boldsymbol{v}}\boldsymbol{u} = \left.\frac{\nabla}{\mathrm{d}t}\boldsymbol{u}(\gamma(t))\right|_{t=0} := \lim_{t\to0}\frac{\Pi_{\gamma(t)\rightsquigarrow p}\boldsymbol{u}(\gamma(t)) - \boldsymbol{u}(p)}{t}, \tag{2.9}$$

where $\Pi_{\gamma(\epsilon)\rightsquigarrow p}$ denotes the inverse of $\Pi_{p\rightsquigarrow\gamma(\epsilon)}$. The covariant derivative, $\nabla : \Gamma(TM)\to\Gamma(TM\otimes T^*M)$, is defined by the relation $\nabla\boldsymbol{u}[\![\boldsymbol{v}]\!] := \nabla_{\boldsymbol{v}}\boldsymbol{u}$ or, in index notation, as $v^i\nabla_i u^j$.

Recall that under a local basis section, $\mathbf{1} \in \Gamma_U(TM)$, where $|\mathbf{1}| = 1$, a tangent vector field $\boldsymbol{u} \in \Gamma_U(TM)$ can be represented as a complex field $\hat{u} : U \to \mathbb{C}$, given by $\boldsymbol{u} = \hat{u}\mathbf{1}$. In this complex representation, the covariant derivative can be expressed as

$$\nabla \boldsymbol{u} = (d\hat{u})\mathbf{1} + \hat{u}(\nabla \mathbf{1}) =: ((d + \mathbf{i}\omega)\hat{u})\mathbf{1}, \tag{2.10}$$

where $d\hat{u} = d\Re(\hat{u}) + \mathbf{i}d\Im(\hat{u}) \in \Gamma_U(T^*M; \mathbb{C})$ represents a complex-valued covector field and ω is a real-valued covector field $\omega \in \Gamma_U(T^*M; \mathbb{R})$ defined by the covariant derivative of the basis field $\nabla \mathbf{1} =: \mathbf{i}\omega\mathbf{1} \in \Gamma_U(TM \otimes T^*M)$. The components of ω are commonly referred to as the Christoffel symbols.

(v) Levi–Civita connection on the nematic bundle

We can extend the Levi–Civita connection from the tangent bundle to the nematic bundle. This is equivalent to defining a nematic covariant derivative, denoted by $\nabla^L : \Gamma(L) \to \Gamma(L \otimes T^*M)$. Under a local nematic basis $[\mathbf{1}] \in \Gamma_U(L)$, the nematic covariant derivative can be defined as

$$\nabla^L[\boldsymbol{q}] = d[\hat{q}]\mathbf{1} + [\hat{q}]\nabla^L[\mathbf{1}] := \left((d + \mathbf{i}2\omega)\,[\hat{q}]\right)[\mathbf{1}], \tag{2.11}$$

where ω is the covector field $\mathbf{i}\omega\mathbf{1} := \nabla\mathbf{1}$ associated with the tangent bundle connection and basis. The nematic connection $\nabla^L[\mathbf{1}] := \mathbf{i}2\omega[\mathbf{1}]$ reflects increased rotational speed due to nematic symmetry. This definition is basis-independent and aligns with the algebraic construction of the Levi–Civita connection on the tangent bundle, $\nabla^L[\boldsymbol{q}] = 2\boldsymbol{q}\nabla\boldsymbol{q} = \nabla(\boldsymbol{q}^2)$.

The nematic covariant derivative $\nabla^L[\boldsymbol{q}]$ is consistent with the standard covariant derivative for matrix-valued functions, $\nabla : \Gamma(TM \otimes TM) \to \Gamma(TM \otimes TM \otimes T^*M)$, when applied to $\boldsymbol{Q} = \mathcal{V}([\boldsymbol{q}]) \in \Gamma(E) \subset \Gamma(TM \otimes TM)$. Via the pushforward of the Veronase map, $d\mathcal{V}|_{[\boldsymbol{q}]} : T_{[\boldsymbol{q}]}\Gamma(L) \to T_{\mathcal{V}([\boldsymbol{q}])}\Gamma(E)$, one can confirm the equivalence of these two derivatives, $\nabla\boldsymbol{Q} = \nabla\boldsymbol{q} \otimes \boldsymbol{q} + \boldsymbol{q} \otimes \nabla\boldsymbol{q} = d\mathcal{V}|_{[\boldsymbol{q}]}[\![\nabla^L[\boldsymbol{q}]]\!]$.

(vi) Laplacian and diffusion

The concept of the covariant derivative naturally leads to a Laplacian operator referred to as the Bochner Laplacian, which is the first variation of the Dirichlet energy.

To begin, we introduce the Bochner Laplacian when it operates on vector fields. The Dirichlet energy functional maps a vector field to an energy measure, $\mathcal{F} : \Gamma(TM) \to \mathbb{R}$, and can be expressed as follows:

$$\mathcal{F}(\boldsymbol{u}) = \frac{1}{2}||\nabla\boldsymbol{u}||^2 \overset{\partial M = \varnothing}{=} \frac{1}{2}\langle\!\langle \boldsymbol{u}, \nabla^*\nabla\boldsymbol{u} \rangle\!\rangle =: -\frac{1}{2}\langle\!\langle \boldsymbol{u}, \Delta\boldsymbol{u} \rangle\!\rangle, \tag{2.12}$$

where the operator $\nabla^* : \Gamma(TM \otimes T^*M) \to \Gamma(TM)$ represents the L_2 adjoint of ∇, defining the Bochner Laplacian as $\Delta := -\nabla^*\nabla : \Gamma(TM) \to \Gamma(TM)$. Note that we use the negative semi-definite convention for the Laplacian operator.

Using the same procedure, the nematic covariant derivative is employed to construct the nematic Dirichlet energy, $\mathcal{F}^L \in \Gamma(L) \to \mathbb{R}$, which is expressed as

$$\mathcal{F}^L([\boldsymbol{q}]) = \frac{1}{2}||\nabla^L[\boldsymbol{q}]||^2 \overset{\partial M = \varnothing}{=} \frac{1}{2}\langle\!\langle [\boldsymbol{q}], \nabla^{L*}\nabla^L[\boldsymbol{q}] \rangle\!\rangle =: -\frac{1}{2}\langle\!\langle [\boldsymbol{q}], \Delta^L[\boldsymbol{q}] \rangle\!\rangle. \tag{2.13}$$

The variation of $\mathcal{F}^L$ leads to the definition of the nematic Bochner Laplacian, denoted as $\Delta^L := -\nabla^{L*}\nabla^L : \Gamma(L) \to \Gamma(L)$.

Analogously, the standard Bochner Laplacian $\Delta : \Gamma(TM \otimes TM) \to \Gamma(TM \otimes TM)$ defined for a general matrix field $\boldsymbol{H}$ can be derived from the matrix Dirichlet energy, $\mathcal{E} : \Gamma(TM \otimes TM) \to \mathbb{R}$, measured by the Frobenius inner product, $\mathcal{E}(\boldsymbol{H}) = (1/2)||\nabla\boldsymbol{H}||^2 = (1/2)\int_M \nabla_i H_{jk}\nabla^i H^{jk}\,\mathrm{d}A$. This Laplacian Δ can act on a nematic field $\boldsymbol{Q} = \mathcal{V}([\boldsymbol{q}])$, but it differs from the nematic Bochner Laplacian, $\Delta\boldsymbol{Q} \neq d\mathcal{V}|_{[\boldsymbol{q}]}[\![\Delta^L[\boldsymbol{q}]]\!]$.

The reason for this difference is twofold. First, nematic fields only correspond to rank-1 matrices in the nematic subspace $E \subset TM \otimes TM$, but the matrix Bochner Laplacian spans the entire $TM \otimes TM$. This results in the matrix representation of nematic fields being an overparametrization under this operator. This overparametrization can be demonstrated by

considering the matrix diffusion equation $\dot{Q} = \Delta Q$. In general, a rank-1 initial condition $Q|_{t=0} \in \Gamma(E)$ does not remain rank-1 under this diffusion (i.e. Q diverges from the nematic subspace E). By contrast, $[\dot{q}] = \Delta^L[q]$ remains within the nematic phase. Second, despite the equivalence of covariant derivatives $\nabla Q = d\mathcal{V}|_{[q]}[\![\nabla^L[q]]\!]$ (cf. §2a(v)), their corresponding Dirichlet energies are distinct: $\mathcal{E}(Q) \neq \mathcal{F}^L([q])$. This is because the pushforward of the Veronese map $\mathrm{d}\mathcal{V}_{[q]} : T_{[q]}L \to T_Q E$ does not isometrically map the intrinsic norm on $T_{[q]}L$ to the Frobenius norm for matrices on $T_Q E$.

As a side remark, it is possible to represent the nematic Dirichlet energy $\mathcal{F}^L([q])$ in terms of Q through an equivalent functional $\mathcal{F}^E : \Gamma(E) \to \mathbb{R}$ such that $\mathcal{F}^E(Q) = \mathcal{F}^L([q])$. We can achieve this by introducing a specific quadratic form, $|\cdot|_Q^2 := |\cdot|^2 - 2\det(\cdot)$, for $\mathbb{R}^{2\times 2}$ matrices on $TM \otimes TM$. This quadratic form induces a corresponding symmetric bilinear form $\langle\cdot,\cdot\rangle_Q = \langle\cdot,\cdot\rangle - 2\det(\cdot,\cdot)$. The equivalent nematic Dirichlet energy $\mathcal{F}^E$ relies on this bilinear form and can be explicitly expressed in index notation

$$\mathcal{F}^E(Q) = \frac{1}{2}\int_M |\nabla Q|_Q^2 \,\mathrm{d}A \equiv \frac{1}{2}\int_M g^{ij}(g_{km}g_{\ell n} - \det(g)\epsilon_{km}\epsilon_{\ell n})\nabla_i Q^{k\ell}\nabla_j Q^{mn}\,\mathrm{d}A. \tag{2.14}$$

Here, g_{ij} are the components of the metric tensor g and ϵ_{ij} represents the Levi–Civita permutation symbol.

In this paper, we adopt the more natural choices of $\mathcal{F}^L([q])$ and Δ^L to model relaxation of the nematic field. We use $\Delta^E : \Gamma(E) \to \Gamma(E)$ to denote the Laplacian equivalent to Δ^L but acting on the matrix field representation. That is, Δ^E satisfies the equivalence $\Delta^E Q = \Delta^E(\mathcal{V}[q]) = \mathrm{d}\mathcal{V}[\![\Delta^L[q]]\!] \in T_Q\Gamma(E)$ and is defined as

$$\Delta^E Q := -\frac{\delta\mathcal{F}^E(Q)}{\delta Q|_E} = -\mathrm{d}\mathcal{V}\left[\!\!\left[\frac{\delta\mathcal{F}([q])}{\delta[q]}\right]\!\!\right] = \mathrm{d}\mathcal{V}\circ\Delta^L\circ\mathcal{V}^{-1}(Q). \tag{2.15}$$

The subscript $|_E$ emphasizes the variation within the nematic subspace E, rather than the entire $TM \otimes TM$.

(vii) Curvature, defects and local-global geometry

The singularities within the nematic field, also referred to as topological defects, are associated with points where the director field exhibits zeros and discontinuities. These defects are commonly characterized by their index or charge $\mathcal{Z}$. To identify these defects and compute their charges, we employ the covariant derivative in closed-loop integration, a classic procedure also discussed in other texts [55,56].

The charge of a topological defect in a k-atic field $[q]_k$ is determined by the cumulative turning angle that the director field undergoes around the defect. Here, we consider a defect at point $p \in U$, where $U \subset M$ represents a sufficiently small disc that does not encircle any other singularities. The boundary of the disc is denoted as $\gamma = \partial U$. Locally in U, it is always possible to establish a smooth and defect-free basis $[\mathbf{1}]_k$ and subsequently express the rotation form under the Levi–Civita connection, denoted as $\eta \in \Gamma(T^*M)$, as

$$\eta := \frac{1}{|[q]_k|^2}\langle\nabla[q]_k, \mathbf{i}[q]_k\rangle = \frac{1}{|[q]_k|^2}\langle \mathrm{d}[q]_k + \mathbf{i}k\omega[q]_k, \mathbf{i}[q]_k\rangle = \mathrm{d}^{\mathbb{S}^1}\arg([\hat{q}]_k) + k\omega. \tag{2.16}$$

Note that the function arg necessitates a smooth basis to be well-behaved and returns values in $\mathbb{S}^1$ rather than real numbers. Despite being $\mathbb{S}^1$-valued by itself, the differential, $d^{\mathbb{S}^1}\arg([\hat{q}]_k)$, can be defined as a real-valued function. This is because, at a given point, this differential depends only on the function's values in a small neighbourhood around the point. In such a local context, a continuous $\mathbb{S}^1$-valued function can be unwrapped to a real-valued function up to a 2π-integer constant that does not affect the differential.

The closed-loop integral of the turning rate η defined in equation (2.16) along the parametrized boundary loop $\gamma(t) = \partial U(t)$, where $t \in [0, T]$ and $\gamma(0) = \gamma(T)$, is referred to as the cumulative turning angle of the director field around a defect. The integral of the connection ω in equation (2.16), which is known as the holonomy angle, is equal to the negative of the integrated

Gaussian curvature: $\oint_\gamma \omega = -\int_U K dA$. Therefore, the charge of the topological defect in a k-atic director field, denoted as $\mathcal{Z} \in \mathbb{Z}/k$, admits the following relation:

$$\mathcal{Z}_p([\boldsymbol{q}]_k) := \frac{1}{2\pi k}\oint_\gamma \mathrm{d}^{\mathbb{S}^1} \arg([\hat{q}]_k) = \frac{1}{2\pi k}\oint_\gamma \eta + \frac{1}{2\pi}\int_U K\,\mathrm{d}A. \tag{2.17}$$

Note that the closed integral ensures that the orientation after integration, $\arg([\hat{q}]_k)|_{t=T}$, differs only by an integer multiple of 2π from its starting value, $\arg([\hat{q}]_k)|_{t=0}$. As a result, the charge is consistently an integer multiple of $1/k$ (i.e. an integer value for a vector field and a multiple of 1/2 for a nematic field). This quantized property also implies that the charge of the defect remains invariant regardless of variations in the size and shape of γ and is solely the property of the director field. As a special case, $\oint_\gamma d^{\mathbb{S}^1} \arg([\hat{q}]_k) = 0$ if γ does not enclose any topological defects of $\arg([\hat{q}]_k)$.

Owing to the Poincaré–Hopf theorem, we can relax the local constraint on U. This theorem relates the sum of charges on the entire manifold M (with $\partial M = \varnothing$) to the topological invariant χ known as the Euler characteristic

$$\sum_i \mathcal{Z}_{p_i}([\boldsymbol{q}]_k) = \chi(M) = 2 - 2g, \tag{2.18}$$

where g represents the genus of the manifold. By replacing U with manifold M, equation (2.17) leads to the Gauss–Bonnet Theorem, which states that the total Gaussian curvature is also a topological invariant, $\int_M K\,\mathrm{d}A = 2\pi\chi(M)$.

In a nutshell, we can detect defects and calculate their charges by establishing the cumulative turning angle through the use of the covariant derivative. Local-to-global theorems, including the Gauss–Bonnet and Poincaré–Hopf theorems, connect local properties such as curvature of the surface and charges of the nematic field to robust global invariants. Practically, as we will elaborate in §3e, these formulae translate to the discretization of Gaussian curvature and the algorithmic computation of topological charges, which satisfy the discrete analogue of local-to-global theorems.

(viii) Expressing the Lie derivative as a covariant derivative

Under the Levi–Civita connection, the Lie derivative can be expressed in terms of the covariant derivative. To demonstrate this, we denote the directional derivative, a derivation associated with its corresponding vector field, as $\boldsymbol{u} := d_{\boldsymbol{u}} : C^\infty(M) \to C^\infty(M)$. In index notation, it is commonly denoted as $u^i\partial_i$. The pullback map respects the derivation structure; for $\boldsymbol{q} \in \Gamma(TM), f \in C^\infty(M)$, we have $\varphi^*(d_{\boldsymbol{q}} f) = d_{\varphi^*\boldsymbol{q}}\varphi^* f$. Consequently, the Lie derivative satisfies the Leibniz rule over derivation, $\mathcal{L}_{\boldsymbol{u}}(d_{\boldsymbol{q}} f) = d_{\mathcal{L}_{\boldsymbol{u}}\boldsymbol{q}} f + d_{\boldsymbol{q}}\mathcal{L}_{\boldsymbol{u}} f$. Since the Lie derivative of a scalar field is equivalent to the directional derivative, we have $\mathcal{L}_{\boldsymbol{u}}\boldsymbol{q}(f) := d_{\mathcal{L}_{\boldsymbol{u}}\boldsymbol{q}} f = \mathcal{L}_{\boldsymbol{u}}(d_{\boldsymbol{q}} f) - d_{\boldsymbol{q}}\mathcal{L}_{\boldsymbol{u}} f = \boldsymbol{u}\boldsymbol{q}(f) - \boldsymbol{q}\boldsymbol{u}(f) =: [\boldsymbol{u}, \boldsymbol{q}](f)$, known as the Lie bracket. The Lie bracket can in fact be expressed using the covariant derivative of the Levi–Civita connection, referred to as the torsion-free condition of the connection, $T^\nabla[\![\boldsymbol{u}, \boldsymbol{q}]\!] := \nabla_{\boldsymbol{u}}\boldsymbol{q} - \nabla_{\boldsymbol{q}}\boldsymbol{u} - [\boldsymbol{u}, \boldsymbol{q}] = 0$. Under the Levi–Civita connection, the Lie material derivative for vector $\boldsymbol{q}$ can be expressed as

$$\dot{\boldsymbol{q}} + \mathcal{L}_{\boldsymbol{u}}\boldsymbol{q} = \dot{\boldsymbol{q}} + \nabla_{\boldsymbol{u}}\boldsymbol{q} - \nabla_{\boldsymbol{q}}\boldsymbol{u}, \tag{2.19}$$

which is a familiar form of the upper-convected derivative, or Oldroyd derivative for vectors [54]. The term $\nabla_{\boldsymbol{u}}\boldsymbol{q}$ represents the parallel transport components, while $\nabla_{\boldsymbol{q}}\boldsymbol{u}$ accounts for the local deformation caused by the differential flow velocity.

Through the pushforward of k-atic equivalence $d[]_k$ (cf. §2a(i)), the Lie derivative of the k-atic director field can be expressed as follows:

$$[\dot{\boldsymbol{q}}]_k + \mathcal{L}_{\boldsymbol{u}}[\boldsymbol{q}]_k = k\boldsymbol{q}^{k-1}(\dot{\boldsymbol{q}} + \mathcal{L}_{\boldsymbol{u}}\boldsymbol{q}), \tag{2.20}$$

where $\boldsymbol{q}^{k-1}$ denotes the $(k-1)$-th power of the nematic $\boldsymbol{q}$ as a complex function. When $k = 2$, this is equivalent to the advection of the tensorial representation of the nematic field. Applying the Leibniz rule of the Lie derivative to the tensor product, we have $\mathcal{L}_{\boldsymbol{u}}\boldsymbol{Q} = \mathcal{L}_{\boldsymbol{u}}\boldsymbol{q} \otimes \boldsymbol{q} + \boldsymbol{q} \otimes \mathcal{L}_{\boldsymbol{u}}\boldsymbol{q}$.

royalsocietypublishing.org/journal/rspa Proc. R. Soc. A 481: 20240418

By rearranging the terms, we recover the operator for the upper-convected derivative of the symmetric tensor $\boldsymbol{Q}$,

$$\begin{aligned}\dot{\boldsymbol{Q}} + \mathcal{L}_{\boldsymbol{u}}\boldsymbol{Q} &= \dot{\boldsymbol{Q}} + \nabla_{\boldsymbol{u}}\boldsymbol{q}\otimes\boldsymbol{q} + \boldsymbol{q}\otimes\nabla_{\boldsymbol{u}}\boldsymbol{q} - \nabla_{\boldsymbol{q}}\boldsymbol{u}\otimes\boldsymbol{q} - \boldsymbol{q}\otimes\nabla_{\boldsymbol{q}}\boldsymbol{u}\\ &= \dot{\boldsymbol{Q}} + \nabla_{\boldsymbol{u}}\boldsymbol{Q} - (\nabla\boldsymbol{u})\boldsymbol{Q} - \boldsymbol{Q}(\nabla\boldsymbol{u}^{\top}).\end{aligned} \tag{2.21}$$

The dual pairing order follows the convention of matrix multiplication (i.e. $(\mathcal{L}_{\boldsymbol{u}}\boldsymbol{Q})^{ij} = u^k\nabla_k Q^{ij} - \nabla_k u^i Q^{kj} - Q^{ik}\nabla_k u^j$ in index notation).

As demonstrated in §2a(iii), the strain rate tensor can be formulated as the Lie derivative of the metric, $\mathcal{L}_{\boldsymbol{u}}\boldsymbol{g}$. When expressing it in terms of the covariant derivative acting on the Eulerian velocity, we can retrieve its well-known form as the symmetric component of the velocity gradient. By expressing $\dot{\boldsymbol{F}} = (\dot{d\varphi}) = \varphi^*(\nabla\dot{\varphi}) = (\nabla\boldsymbol{u})\boldsymbol{F} \in \Gamma(TM\otimes T^*M)$, we can express the Lie derivative of the metric as the pullback of the strain rate tensor,

$$\mathcal{L}_{\boldsymbol{u}}\boldsymbol{g} = \frac{\partial}{\partial t}(\boldsymbol{F}^{\top}\boldsymbol{g}\boldsymbol{F}) = \dot{\boldsymbol{F}}^{\top}\boldsymbol{g}\boldsymbol{F} + \boldsymbol{F}^{\top}\boldsymbol{g}\dot{\boldsymbol{F}} = \boldsymbol{F}^{\top}(\nabla\boldsymbol{u}^{\top}\boldsymbol{g} + \boldsymbol{g}\nabla\boldsymbol{u})\boldsymbol{F} = \varphi^*(\nabla\boldsymbol{u}^{\top}\boldsymbol{g} + \boldsymbol{g}\nabla\boldsymbol{u}). \tag{2.22}$$

Since the flowmap, $\varphi : M \to M$, is instantaneously an identity map, we have $\mathcal{L}_{\boldsymbol{u}}\boldsymbol{g} = \nabla\boldsymbol{u}^{\top}\boldsymbol{g} + \boldsymbol{g}\nabla\boldsymbol{u} \in \Gamma(T^*M\otimes_{\mathrm{symm}} T^*M)$, which measures the infinitesimal deformation rate of a fluid element. This Lie derivative defines the Killing operator,

$$\mathcal{K} : \Gamma(TM) \to \Gamma(T^*M\otimes_{\mathrm{symm}} T^*M), \quad \mathcal{K} : \boldsymbol{u} \mapsto \frac{1}{2}\mathcal{L}_{\boldsymbol{u}}\boldsymbol{g}. \tag{2.23}$$

A vector field $\boldsymbol{v}$ is referred to as a Killing vector field if $\mathcal{K}\boldsymbol{v} = 0$ (i.e. the flow it generates preserves the metric).

(b) Hydrodynamics of active nematic films

In this section, we will extend the mathematical framework from the previous sections to describe the hydrodynamics of an active nematic film on a curved surface. The system can be analysed in two parts. First, we have the steady-state Stokes equations, which describe how the fluid responds to the active stress induced by the nematic configuration. Subsequently, the steady-state fluid velocity acts as the driving force for the nematodynamics equation, an advection–diffusion equation that governs the behaviour of the nematic field. The system assumes quasi-static coupling, meaning that the dissipation in the fluid at this length scale is considered instantaneous.

(i) Forced surface Stokes flow

We focus on an active nematic confined to a fluid interface, where the flow is governed by the two-dimensional overdamped Stokes equations. Bulk fluid effects are not explicitly modelled, which is valid when surface dissipation dominates over bulk dissipation (i.e. when the Saffman–Delbrück length far exceeds the system size) [57,58]. The dynamics of such dissipation-driven systems can be systematically derived using the Onsager variational principle [42,57,59–62]. The associated functional, known as the Rayleighian, captures the dissipation rate of the system, and Stokes flow emerges as the stationary condition of this dissipation function. In this work, we consider only viscous dissipation, neglecting reactive stresses from nematic elasticity in advection (cf. §2a(ii) and [63]). The fluid flow is driven by the active nematic stress $\boldsymbol{\sigma} = \alpha\boldsymbol{Q} \in \Gamma(TM\otimes_{\mathrm{symm}} TM)$, which aligns with the orientation of the nematic constituents and can be either contractile ($\alpha > 0$) or extensile ($\alpha < 0$) [64]. The assumption of an active stress-dominant regime is valid in many practical cases [2,65].

The formulation of Stokes flow involves minimizing the Rayleighian while satisfying the incompressibility constraint,

$$\min_{\boldsymbol{u}} \quad \mu\langle\!\langle\mathcal{K}\boldsymbol{u},\mathcal{K}\boldsymbol{u}\rangle\!\rangle - \langle\!\langle\boldsymbol{u},\mathrm{div}^{\nabla}\boldsymbol{\sigma}\rangle\!\rangle \quad \text{subject to} \quad \mathrm{div}\,\boldsymbol{u} = 0, \tag{2.24}$$

where the first term $\mu\langle\!\langle \mathcal{K}\boldsymbol{u}, \mathcal{K}\boldsymbol{u}\rangle\!\rangle$ quantifies the rate of viscous dissipation [31,32,41]. Here, the divergence operator, $\mathrm{div} := -\mathrm{grad}^* : \Gamma(TM) \to C^\infty$, is the negated L_2 adjoint of the gradient operator, $\mathrm{grad} := \boldsymbol{g}^{-1}d : C^\infty \to \Gamma(TM)$.

The negated adjoint of the covariant derivative is referred to as the covariant divergence, $\mathrm{div}^\nabla := -\nabla^* : \Gamma(TM \otimes TM) \to \Gamma(TM)$.

The Killing operator $\mathcal{K}$ can be decomposed using the covariant *del bar* opeartor $\bar{\partial}^\nabla$ as $\mathcal{K}\boldsymbol{u} = \bar{\partial}^\nabla \boldsymbol{u} + \mathrm{div}(\boldsymbol{u})\boldsymbol{I}/2$. Here, $\bar{\partial}^\nabla \boldsymbol{u}$ quantifies the degree of non-conformality or infinitesimal shearing induced by the velocity field. The remaining term, $\mathrm{div}(\boldsymbol{u})\boldsymbol{I}/2$, characterizes isotropic fluid dilation. For a detailed discussion of the holomorphic structure, including the definitions of covariant *del* ∂^∇ and *del bar* $\bar{\partial}^\nabla$ operators and their relevance in fluid mechanics, see electronic supplementary material, S1. Under incompressibility, we can replace $\mathcal{K}$ with $\bar{\partial}^\nabla$ and represent the constrained optimization problem as a mini–max problem:

$$\min_{\boldsymbol{u}} \max_{p} \mathcal{R} = \mu\langle\!\langle \bar{\partial}^\nabla \boldsymbol{u}, \bar{\partial}^\nabla \boldsymbol{u}\rangle\!\rangle - \langle\!\langle \boldsymbol{u}, \mathrm{div}^\nabla \boldsymbol{\sigma}\rangle\!\rangle - \langle\!\langle p, \mathrm{div}\, \boldsymbol{u}\rangle\!\rangle. \tag{2.25}$$

In this expression, p is the fluid pressure acting as a Lagrange multiplier for incompressibility. On a closed surface with $\partial M = \varnothing$, the stationary conditions with respect to velocity $\boldsymbol{u}$ and pressure p yield the incompressible, steady Stokes equations on a two-dimensional Riemannian manifold

$$\begin{aligned} 2\mu\ \bar{\partial}^{\nabla *}\bar{\partial}^\nabla \boldsymbol{u} + \mathrm{grad}\ p - \alpha\ \mathrm{div}^\nabla \boldsymbol{Q} &= 0, \\ \mathrm{div}\ \boldsymbol{u} &= 0. \end{aligned} \tag{2.26}$$

The curvature contributes to the viscous term as $-2\bar{\partial}^{\nabla *}\bar{\partial}^\nabla \boldsymbol{u} = (\Delta + K)\boldsymbol{u}$. This result can be deduced from the known approach based on Riemannian geometry that results in the relation $-2\mathcal{K}^*\mathcal{K}\boldsymbol{u} = (\Delta + K + \mathrm{grad}\,\mathrm{div})\boldsymbol{u}$ [26,31,32]. In addition, in electronic supplementary material, S1.1, we provide an alternative derivation within the framework of complex manifolds using complex differential forms.

Note that the existence of a Killing vector field indicates symmetries in the geometry, such as the rigid body rotation on a rotationally symmetric surface. In such case, the Stokes equations might lack full rank, leading to non-unique solutions with a kernel represented by the Killing vector field. In our study, we select the least-norm solution as the canonical one to the Stokes equations. This choice is equivalent to projecting out all modes of Killing fields in the L_2 sense. The treatment is justified by the following. In theory, the L_2 Killing component of the velocity does not contribute to energy dissipation, and as a result, it remains conserved in the presence of any non-zero inertia. This is an instance of Noether's theorem, which states that the presence of continuous spatial symmetry, represented by a Killing vector field, implies the conservation of momentum. Therefore, in such an ideal case, the correct solution is the least-norm solution with the addition of the Killing mode in the initial condition. However, in practical situations, particularly when considering an interfacial fluid surface that separates two bulk viscous fluids, the Killing mode will eventually dissipate energy through frictional interactions with the substrate.[1] In this case, the system should converge to the least-norm solution over time. In §3b, we will elaborate on the implementation of the Killing projection.

(ii) Nematodynamics

Modelling nematodynamics involves studying the dynamics of nematic liquid crystals, which possess both fluid-like and orientational order properties. In this study, we are particularly interested in the sharply aligned limit of the active nematic field. This sharply aligned phase arises when the microscopic rotational diffusion of the nematic molecules is negligible compared with steric alignment [66]. Under these conditions, the nematodynamics of the macroscopic order parameter becomes identical to the dynamics of individual microscopic nematic filaments. A commonly used approach is to use an advection–diffusion equation, where advection accounts for the flow-induced alignment and rotation of the nematic director field, while diffusion represents

[1]Interactions with the bulk fluid are not considered in this study.

the smoothing of the director due to random molecular interactions [23]. There are various convective rates and models proposed for describing nematic advection and flow alignment [14,67,68]. In this work, we model the advection of nematic molecules based on Jeffery's microphysical theory [66,69] and express it using the Lie derivative framework. The numerical scheme for this convective rate is detailed in §3b and can be easily adapted to other used rates.

The relaxation or diffusion part of the nematodynamics equation involves the nematic Bochner Laplacian established in §2a(vi). The constraint $|[\boldsymbol{q}]| = 1$ imposes the sharply aligned phase. However, according to the Poincaré–Hopf theorem, zeros of the director field are guaranteed unless the system is on a torus with a vanishing Euler characteristic $\chi = 0$ (cf. §2a(vii)). To address this constraint, we adopt a Landau–de Gennes formulation and introduce a weak constraint through a penalizing energy term $\mathcal{G}([\boldsymbol{q}]) = (|[\boldsymbol{q}]|^2 - 1)^2/(4\varepsilon^2)$ in addition to the Dirichlet energy $|\nabla^L[\boldsymbol{q}]|^2/2$. Here, ε represents the coherence length scale around the defects [30]. Together, these terms are referred to as the Frank–Oseen energy [70–74], the gradient flow of which induces a diffusion. Note that the nematodynamics in the close vicinity of defects is not captured by the present model and requires more detailed analysis [75]. Furthermore, this minimal model for nematic elasticity does not include the alignment effects induced by extrinsic geometry [76,77], nor does the complex representation account for out-of-plane components of nematic fields [78].

The advection of nematic molecules is captured by a combination of an adapted isometric Lie transportation and the 'rotation-only' Lie transportation. Lie transportation, as described in §2a(iii), models how the nematic director field is passively transformed by the flow generated by a velocity field. The rotation-only Lie transportation factors out the stretching part of the Lie transportation, and thus a nematic director is only rotated while keeping its magnitude.

By decomposing the velocity gradient into symmetric ($\boldsymbol{E} = \mathcal{K}\boldsymbol{u}$, representing strain rate) and skew-symmetric ($\boldsymbol{W} = \nabla\boldsymbol{u} - \boldsymbol{E}$, representing vorticity) components, we can express the nematic Lie derivative (cf. equation (2.8) and §2a(viii)) as $\mathcal{L}_{\boldsymbol{u}}[\boldsymbol{q}] = 2\boldsymbol{q}\mathcal{L}_{\boldsymbol{u}}\boldsymbol{q}$, where $\mathcal{L}_{\boldsymbol{u}}\boldsymbol{q} = \nabla_{\boldsymbol{u}}\boldsymbol{q} - \boldsymbol{E}\boldsymbol{q} - \boldsymbol{W}\boldsymbol{q}$. The vorticity $\boldsymbol{W}$ and the parallel transport $\nabla_{\boldsymbol{u}}$ contribute to infinitesimal rotational transformations that preserve length, whereas the strain rate $\boldsymbol{E}$ affects the molecules by aligning them with the flow and causing axial stretching or compression.

A rotational Lie derivative, $\mathcal{L}^{\mathrm{rot}}_{\boldsymbol{u}}$, also known as the Jaumann or corotational derivative, specifically focuses on the rotation effect induced by the flow, (e.g. $\mathcal{L}^{\mathrm{rot}}_{\boldsymbol{u}}\boldsymbol{q} = \nabla_{\boldsymbol{u}}\boldsymbol{q} - \boldsymbol{W}\boldsymbol{q}$ for vector fields $\boldsymbol{q}$). Like the classical Lie derivatives (§2a(iii)), the rotational Lie derivative $\mathcal{L}^{\mathrm{rot}}_{\boldsymbol{u}}$ is defined through a pullback operation. The only difference is that this pullback is only the rotation component of the classical pullback operator. Recall from equation (2.7) that if φ is a flow map with deformation gradient $\boldsymbol{F}$, the pullback of a vector field and, respectively, a nematic field is given by $\varphi^*\boldsymbol{q} = \boldsymbol{F}^{-1}\boldsymbol{q}$, $\varphi^*[\boldsymbol{q}] = [\boldsymbol{F}^{-1}\boldsymbol{q}]$ and $\varphi^*\boldsymbol{Q} = \boldsymbol{F}^{-1}\boldsymbol{Q}\boldsymbol{F}^{-\top}$. Now, let $\boldsymbol{R}$ denote the rotational component of $\boldsymbol{F}$ in the polar decomposition $\boldsymbol{F} = \boldsymbol{R}\boldsymbol{U}$. Define the *rotational pullback* φ^*_{rot} on vector fields and nematic fields by $\varphi^*_{\mathrm{rot}}\boldsymbol{q} := \boldsymbol{R}^{-1}\boldsymbol{q}$, $\varphi^*_{\mathrm{rot}}[\boldsymbol{q}] := [\boldsymbol{R}^{-1}\boldsymbol{q}]$, and $\varphi^*_{\mathrm{rot}}\boldsymbol{Q} := \boldsymbol{R}^{-1}\boldsymbol{Q}\boldsymbol{R}^{-\top}$. Via this rotational pullback operator, define the Jaumann derivative as $\mathcal{L}^{\mathrm{rot}}_{\boldsymbol{u}} := \partial/\partial t \circ \varphi^*_{\mathrm{rot}}$, where φ is the infinitesimal flow map generated by $\boldsymbol{u}$. In terms of the gradients $\nabla\boldsymbol{u}$, $\boldsymbol{E}$, $\boldsymbol{W}$ of $\boldsymbol{u}$,

$$\mathcal{L}^{\mathrm{rot}}_{\boldsymbol{u}}\boldsymbol{q} = \nabla_{\boldsymbol{u}}\boldsymbol{q} - \boldsymbol{W}\boldsymbol{q}, \quad \mathcal{L}^{\mathrm{rot}}_{\boldsymbol{u}}[\boldsymbol{q}] = 2\boldsymbol{q}\mathcal{L}^{\mathrm{rot}}_{\boldsymbol{u}}\boldsymbol{q}, \quad \mathcal{L}^{\mathrm{rot}}_{\boldsymbol{u}}\boldsymbol{Q} = \nabla_{\boldsymbol{u}}\boldsymbol{Q} - \boldsymbol{W}\boldsymbol{Q} + \boldsymbol{Q}\boldsymbol{W}. \tag{2.27}$$

The combination of the Jaumann derivative with the traditional Lie derivative in a weighted manner, denoted as $\mathcal{L}^{\lambda}_{\boldsymbol{u}} := \lambda\mathcal{L}_{\boldsymbol{u}} + (1-\lambda)\mathcal{L}^{\mathrm{rot}}_{\boldsymbol{u}}$, $\lambda \in [0,1]$, allows for the modelling of nematic particles with different aspect ratios. The parameter $\lambda \in [0,1]$ allows for a linear transition from considering the full velocity gradient at $\lambda = 1$ to only the spin tensor at $\lambda = 0$. In the literature, the non-dimensional parameter λ is referred to as the tumbling parameter or Bretherton's constant and determines the dominance of alignment in extensional flow versus tumbling in rotational flow [79,80].

In addition, nematic molecules are inextensible when subjected to flow. During advection, the magnitude of the order parameter is transported like a scalar field without undergoing stretching. Therefore, we project out the stretching component in the Lie derivatives $\mathcal{L}^{\lambda}_{\boldsymbol{u}}$. Explicitly, the

projected Lie derivatives are given by

$$\mathcal{P}(\mathcal{L}_u^\lambda q) := \mathcal{L}_u^\lambda q - \frac{1}{|q|^2}\langle \mathcal{L}_u^\lambda q, q\rangle q = \nabla_u q - Wq - \lambda Eq + \frac{\lambda}{|q|^2}\langle Eq, q\rangle q,$$

$$\mathcal{P}^L(\mathcal{L}_u^\lambda [q]) := \mathcal{L}_u^\lambda [q] - \frac{1}{|[q]|^2}\langle \mathcal{L}_u^\lambda [q], [q]\rangle [q] = 2q\,\mathcal{P}(\mathcal{L}_u^\lambda q)$$

and

$$\mathcal{P}^E(\mathcal{L}_u^\lambda Q) := \mathcal{L}_u^\lambda Q - \frac{1}{|Q|^2}\langle \mathcal{L}_u^\lambda Q, Q\rangle Q,$$

$$= \nabla_u Q - (\lambda E + W)Q - Q(\lambda E - W) + \frac{2\lambda}{|Q|}\langle E, Q\rangle Q. \tag{2.28}$$

Here, we normalize Q based on the Frobenius matrix product $\langle\cdot,\cdot\rangle$. It is equally valid to use the nematic norm $\langle\cdot,\cdot\rangle_{\mathcal{Q}}$ introduced in equation (2.14). Projections based on both norms are equivalent because $\det(Q) = 0$, meaning $|Q| = |Q|_{\mathcal{Q}}$, and $2\det(Q, Q') = \det(Q, Q)' = \det(Q)' = 0$, indicating $\langle Q', Q\rangle = \langle Q', Q\rangle_{\mathcal{Q}}$. In the literature, the generalized isometric advection equation based on equation (2.28) is known as Jeffery's equation [69].

By combining Jeffery advection with the Ginzburg–Landau diffusion, we obtain the nematodynamics equations governing the evolution of the surface nematic

$$\left.\begin{aligned} \dot{[q]} + \mathcal{P}^L(\mathcal{L}_u^\lambda [q]) &= \frac{1}{\eta}\left(\Delta^L [q] - \frac{\delta \mathcal{G}}{\delta [q]}\right) \\ \text{and}\qquad \dot{Q} + \mathcal{P}^E(\mathcal{L}_u^\lambda Q) &= \frac{1}{\eta}\left(\Delta^E Q - d\mathcal{V}\left[\!\left[\frac{\delta \mathcal{G}}{\delta [q]}\right]\!\right]\right), \end{aligned}\right\} \tag{2.29}$$

where

$$\frac{\delta \mathcal{G}([q])}{\delta [q]} = \frac{1}{\varepsilon^2}(|[q]|^2 - 1)[q], \tag{2.30}$$

and η is the so-called rotational viscosity (distinct from the microscopic rotational diffusion). Although not explicitly apparent, the Gaussian curvature K plays an implicit role in the Bochner Laplacian through the Levi–Civita connection [26,47].

(iii) System of equations

We summarize and non-dimensionalize the governing equations for the hydrodynamics of an active nematic fluid film. Using the domain length scale, denoted as r, as the characteristic length scale and the time scale $\tau = \mu|\alpha|^{-1}$, we can scale all variables and differential operators. This leads to the dimensionless system given by

$$(\Delta + K)\boldsymbol{u} - \operatorname{grad} p \pm \operatorname{div}^\nabla Q = 0, \quad \operatorname{div} \boldsymbol{u} = 0 \tag{2.31a}$$

and

$$\dot{[q]} + \mathcal{P}^L \mathcal{L}_u^\lambda [q] = \frac{1}{Pe}\left(\Delta^L [q] - \frac{1}{\epsilon^2}(|[q]|^2 - 1)[q]\right), \tag{2.31b}$$

where $\lambda \in [0, 1]$ is the tumbling parameter; $Pe = |\alpha|\eta r^2 \mu^{-1}$ is the active Peclet number, which measures the influence of activity-driven Jeffery advection compared with nematic relaxation; $\epsilon = \varepsilon/r$ characterizes the size of a defect core by comparing the coherence length to the system size. Throughout the rest of the study, we solve the non-dimensional version of the system. In the numerical results presented below, we assume the limit $\epsilon \to 0$ and adopt a normalization procedure to account for the Ginzburg–Landau term.

3. Discretization and algorithm

In this section, we will explain the construction of a discrete system for modelling an active fluid on a two-dimensional triangular manifold mesh. We solve equation (2.31) by

time splitting (cf. algorithm 1). At each time step, the active force is calculated by taking the covariant divergence of the stress tensor induced by the nematic field. This active force gives rise to a fluid velocity field, which is obtained by solving the discrete Stokes equations (equation (2.31*a*)) through augmented-Lagrangian (AL) iteration. Next, the nematodynamics equation (equation (2.31*b*)) evolves the nematic field with the advection by the Stokes flow velocity field, as well as the relaxation. The advection and relaxation terms are separated in a splitting procedure. We first compute the evolution of the nematic field Lie-advected by the velocity using an explicit semi-Lagrangian (sL) scheme. The one-step relaxation, based on the Bochner Laplacian operator, is solved using the implicit Euler method to ensure unconditional stability. The projection that removes the stretching component of the Lie derivative and the constraint imposed by the Ginzburg–Landau term are consolidated into a single normalization step. For completeness, we also include a discrete counterpart of the theory of §2a(vii) about curvature and defects, enabling us to determine the locations and charges of the topological defects. The discretization presented in this work offers several distinctive features:

— The calculations are carried out on a two-dimensional triangular mesh, rather than a volumetric grid, allowing for efficient and accurate representation of the system.
— Tensor fields and differential operators are intrinsically represented using the discrete complex line bundle. This representation, in contrast to the common approach of applying extra tangentiality constraints on Euclidean tensors and operators, allows better accuracy and lower computational cost.
— A generalized sL method is employed to handle the Lie derivative for both vector and tensor quantities, thereby providing a general procedure for the advection of *k*-atic directors.
— We use isomorphic representations of the nematic field through the Veronese map. This allows us to adapt to the more convenient representation at each stage of the algorithm.

In addition to the theoretical and algorithmic development, we provide an implementation using SideFX Houdini with the VEX language and Python module (see electronic supplementary material, S2 for a brief introduction to the software). Our implementation is accessible through a public repository on GitHub: https://is.gd/5VpfIf.

Algorithm 1. Hydrodynamics of active nematics.

Inputs:
  Surface M, curvature K, time step Δt
Initialize:
  Nematic field $Q = \mathcal{V}([q])$
for $t = 0$ to T **do**
  STOKES FLOW(Q)
    $f \leftarrow \mathrm{div}^{\nabla} Q$
    $u, p \leftarrow$ SOLVE($(\Delta + K)u = \mathrm{grad}\, p - f, \mathrm{div}\, u = 0$) ▷ AL iteration (§3f)
  NEMATODYNAMICS(u, Q)
    $Q \leftarrow$ SOLVE($\dot{Q} + \mathcal{P}^E \mathcal{L}_u^{\lambda} Q = 0$) ▷ Explicit sL (§3b)
    $[q] \leftarrow \mathcal{V}^{-1}(Q)$
    $[q] \leftarrow$ SOLVE($[\dot{q}] = Pe^{-1} \Delta^L [q]$) ▷ Implicit Euler
    $Q \leftarrow \mathcal{V}$(NORMALIZE($[q]$))
    $t \leftarrow t + \Delta t$
end for

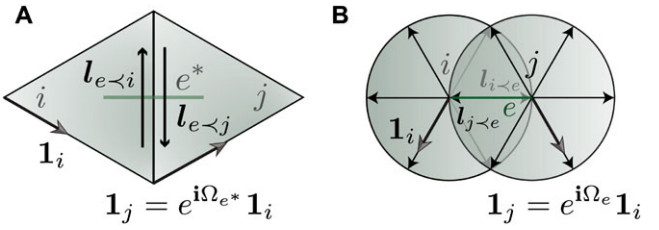

Figure 1. Schematics depicting intrinsic parallel transport on a two-dimensional triangular mesh: (a) face–face transportation by flattening the dihedral angle within a two-triangle stencil. (b) vertex–vertex transportation preserves angles along geodesic paths within the geodesic polar map.

(a) Discrete manifold and choice of variable space

In this section, our goal is to establish the discrete Levi–Civita connection (§3a(i)) on a discrete triangular mesh and specify the choice of the space of discretization variables (§3a(ii)) for the active nematic system. The notation for mesh navigation is standard in the literature [49] and likely to be clear from the context. To aid the reader, we have also included self-contained introductory materials in electronic supplementary material, S2 for an audience unfamiliar with the notation.

(i) Levi–Civita connection

We equip the discrete manifold with a Levi–Civita connection (cf. §2a(iv)) by locally constructing the discrete parallel transport. This includes the parallel transport from the tangent space of one vertex to its neighbouring vertex, from a face to its neighbouring face, as well as from a vertex to its neighbouring face. The construction of a discrete Levi–Civita connection follows common approaches in discrete differential geometry and design of k-RoSy fields [47–49].

The face–face and vertex–vertex transportations can be defined intrinsically (i.e. invariant under isometric deformation). Therefore, parallel transport of a vector $\boldsymbol{u}$ from face f_i to face f_j along the dual edge e^*, where $e \prec f_i, f_j$, can be conceptualized as if the dihedral angle at e were flattened (cf. figure 1a). In this context, parallel transport simplifies to a basis change across face f_i to face f_j,

$$\Pi_{i\rightsquigarrow j} : T_{f_i}M \to T_{f_j}M, \quad \Pi_{i\rightsquigarrow j}(\boldsymbol{u}_i) = \Pi_{i\rightsquigarrow j}(\hat{u}_i\mathbf{1}_i) = e^{-\mathbf{i}\Omega_{e^*}}\hat{u}_i\mathbf{1}_j. \tag{3.1}$$

The vertex–vertex parallel transport is intrinsically defined by maintaining the angle with respect to the connecting edge e between neighbouring vertices $v_i, v_j \prec e$, illustrated by figure 1b. As seen in §2a(v), the nematic field requires amplifying the Levi–Civita connection on the tangent bundle Ω to 2Ω. Subsequently, we can express the parallel transport of a nematic director $[\boldsymbol{q}]_i \in L_{v_i}$ to L_{v_j} along $\boldsymbol{l}_e$ as

$$\Pi_{i\rightsquigarrow j} : L_{v_i} \to L_{v_j} \quad \text{and} \quad \Pi_{i\rightsquigarrow j}([\boldsymbol{q}]_i) = \Pi_{i\rightsquigarrow j}([\hat{q}]_i[\mathbf{1}]_i) = e^{-\mathbf{i}2\Omega_e}[\hat{q}]_i[\mathbf{1}]_j. \tag{3.2}$$

Here, the primal edge connection, $\Omega_e = \arg(\boldsymbol{l}_{v_j\prec e}) - \arg(\boldsymbol{l}_{v_i\prec e}) - \pi$, quantifies the basis change across $T_{v_i}M$ and $T_{v_j}M$ (cf. figure 1b).

The vertex–face transportation is achieved using the $\mathbb{R}^3$ embedding. Given the embedding of the mesh and the realization of the tangent vector in $\mathbb{R}^3$, we can use a three-dimensional dihedral rotation to map from one vertex tangent space to a neighbouring face tangent space and vice versa (cf. the continuous theory in §2a(iv)). To illustrate this, consider a vertex unit normal, $\boldsymbol{n}_v \in T_v^{\perp}M, |\boldsymbol{n}_v| = 1$, and a face unit normal, $\boldsymbol{n}_f \in T_f^{\perp}M$, $|\boldsymbol{n}_v| = 1$. The dihedral rotation from $\boldsymbol{n}_v$ to $\boldsymbol{n}_f$ is defined as the rotation $\boldsymbol{R}_{vf}$ with angle $\cos^{-1}\langle \boldsymbol{n}_v, \boldsymbol{n}_f\rangle$ about the axis $\boldsymbol{l} = \boldsymbol{n}_v \times \boldsymbol{n}_f/|\boldsymbol{n}_v \times \boldsymbol{n}_f|$. Define $\Pi_{v\rightsquigarrow f} := \boldsymbol{R}_{vf} : T_vM \to T_fM$. Note that the definition of $\boldsymbol{n}_v$ is not unique. In practice, we use an angle-weighted vertex normal $\boldsymbol{n}_v := (\sum_{f\succ v} \tilde{\angle}_{f\succ v}\boldsymbol{n}_f)/(2\pi)$.

(ii) Space of system variables and operator mappings

In this section, we specify the choice of space where the discretization variable resides, and the mapping spaces imposed by the differential operators. In §§ 3b–d, we will recapitulate the specific definitions of the operators.

In our approach, we discretize the Stokes equations on the faces of the mesh and the nematodynamics equation on the vertices. Specifically, we work with a face-based fluid velocity denoted as $\boldsymbol{u} \in \Gamma_{\mathfrak{F}}(TM)$ and a vertex-based nematic director represented as $[\boldsymbol{q}] \in \Gamma_{\mathfrak{V}}(L)$, alongside the corresponding matrix representation $\boldsymbol{Q} = \boldsymbol{q} \otimes \boldsymbol{q} \in \Gamma_{\mathfrak{V}}(E)$.

Subsequently, we develop the discrete differential operators associated with these choices. For the Stokes equations, we construct the Bochner Laplacian $\Delta : \Gamma_{\mathfrak{F}}(TM) \to \Gamma_{\mathfrak{F}}(TM)$ based on the face–face Levi–Civita connection. The gradient operator, $\mathrm{grad} : C_{\mathfrak{V}}(M) \to \Gamma_{\mathfrak{F}}(TM)$, maps scalar vertex data to vector face data. The divergence operator, the adjoint of the gradient, maps vectors from faces to scalar measurements at vertices, $\mathrm{div} : \Gamma_{\mathfrak{F}}(TM) \to C_{\mathfrak{V}}(M)$. Similarly, for the nematodynamics equation, we establish the nematic Bochner Laplacian $\Delta^L[\boldsymbol{q}] : \Gamma_{\mathfrak{V}}(L) \to \Gamma_{\mathfrak{V}}(L)$ using the vertex–vertex Levi–Civita connection. We also introduce a vertex-based Lie derivative $\mathcal{L}_{\boldsymbol{u}} : \Gamma_{\mathfrak{V}}(E) \to \Gamma_{\mathfrak{V}}(E)$ to advect the nematic director.

(b) sL Lie advection and nematodynamics

The sL method is an explicit space–time integrator for advection equations similar to an upwinding scheme [81]. Here, we introduce the sL method generalized to any Lie advection equation for tensor fields as follows. Given a velocity field, we construct a backward flowmap by tracing the velocity field upwind. This flowmap is used to pullback the tensor field from the previous time step as the update rule. The principle can be applied to tensors of arbitrary (r, s) type (e.g. the valence-k tensor that represents the k-atic field [14]), serving as a discrete counterpart to the continuous theory discussed in §2a(iii). The resultant scheme, summarized in algorithm 2, captures the geometric structure of nematic advection and enhances numerical stability.

Concretely, given a time-independent velocity field $\boldsymbol{u} \in \Gamma_{\mathfrak{V}}(TM)$, we construct a finite-time backward flowmap $\Psi_{\Delta t}$ by integrating the ODE, $\partial_\tau \Psi_\tau = -\boldsymbol{u}(\Psi_\tau)$, $\tau \in [0, \Delta t]$, with the initial condition $\Psi_0 = \mathrm{id}_M$. In practice, we represent Ψ_τ and $\boldsymbol{u}$ as $\mathbb{R}^3$-valued functions using surface embeddings and implement the integration using RK4. To evaluate $\boldsymbol{u} \circ \Psi_\tau$, we use a closest-point projection followed by a linear interpolation in a triangle. Recall in the continuous setting that Lie advection $\partial_t[\boldsymbol{q}] + \mathcal{L}_{\boldsymbol{u}}[\boldsymbol{q}] = 0$ is characterized by a constant pullback field $\partial_t \varphi^*[\boldsymbol{q}] = 0$ (cf. equation (2.8)). With the backward flowmap $\Psi_{\Delta t}$ and its gradient $d\Psi_{\Delta t}$, a discrete Lie advection is analogously represented by updating the nematic field $[\boldsymbol{q}]$ using its pullback value $\Psi^*_{\Delta t}[\boldsymbol{q}]$. The procedure will be made explicit in following subsections.

(i) Deformation gradient of backward flowmap

By evaluating the finite-time flowmap over vertices (i.e. $\Psi_{\Delta t}$ such that $M_{\Delta t} = \Psi_{\Delta t} M$), we can construct the deformation gradient $d\Psi_{\Delta t}|_f$ (realized in $\mathbb{R}^3$) on each triangle face f as follows:

$$\mathrm{d}\Psi_{\Delta t} : \Gamma_{\mathfrak{F}}(TM) \to \Gamma_{\mathfrak{F}}(T_{\Psi_{\Delta t}} M_{\Delta t}) \quad \text{and} \quad \mathrm{d}\Psi_{\Delta t}|_f := \begin{bmatrix} | & | & | \\ \boldsymbol{l}_1 & \boldsymbol{l}_2 & \boldsymbol{n} \\ | & | & | \end{bmatrix}_{\Psi_{\Delta t}(f)} \begin{bmatrix} | & | & | \\ \boldsymbol{l}_1 & \boldsymbol{l}_2 & \boldsymbol{n} \\ | & | & | \end{bmatrix}_f^{-1}. \tag{3.3}$$

These column vectors, illustrated by figure 2, represent the embedded edge vectors $\boldsymbol{l} \in \mathbb{R}^3$ and the unit face normal $\boldsymbol{n} \in \mathbb{R}^3$ before and after the backward flowmap $\Psi_{\Delta t}$. A vertex-based deformation gradient $\boldsymbol{F} : \Gamma_{\mathfrak{V}}(TM) \to \Gamma_{\mathfrak{V}}(T_{\Psi_{\Delta t}} M_{\Delta t})$ is obtained by averaging the deformation gradient on incident faces, $\boldsymbol{F}|_v = (1/|f \succ v|) \sum_{f \succ v} d\Psi_{\Delta t}|_f$.

(ii) Pullback of the nematic field

Recall that the nematic field can be equivalently expressed using the matrix representation $\boldsymbol{Q} = \mathcal{V}([\boldsymbol{q}]) \in \Gamma_{\mathfrak{V}}(TM \otimes TM)$. With $\boldsymbol{Q}$ realized as an $\mathbb{R}^{3\times 3}$-valued function, its Lie advection,

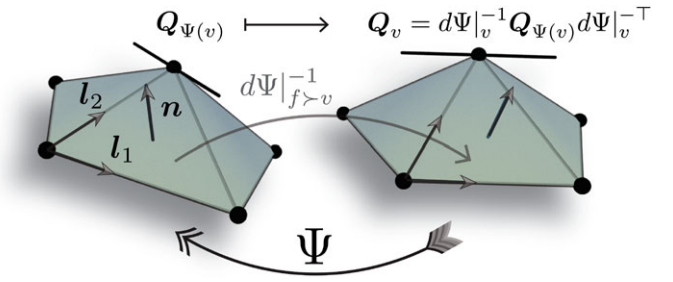

Figure 2. The sL Lie advection is performed on a triangular mesh using a backward finite time flowmap Ψ. This flowmap engenders a piecewise constant deformation gradient $d\Psi|_{f\succ v}$ defined over the triangle faces. By averaging this face-based deformation gradient around the one-ring neighbourhood of each vertex, we derive a vertex-based deformation gradient $d\Psi|_v$. The nematic Lie advection is modelled by updating Q_v with $d\Psi|_v^{-1} Q_{\Psi(v)} d\Psi|_v^{-\top}$.

$\partial_t Q + \mathcal{L}_u Q = 0$, with $t \in [0, \Delta t]$, $Q|_{t=0} = Q_0$, can be modelled by

$$Q_{\Delta t} = \Psi_{\Delta t}^* Q_0 = F^{-1}(Q_0 \circ \Psi_{\Delta t}) F^{-\top}, \tag{3.4}$$

where $Q_{\Delta t}$ denotes the updated value of Q for the subsequent time step. Because the backward flowmap $\Psi_{\Delta t}$ can land anywhere on M, evaluating $Q_0 \circ \Psi_{\Delta t}$ requires interpolation, such as trilinear interpolation using the face-barycentric representation of $\Psi_{\Delta t}$. However, this interpolation may not preserve the rank-1 structure of Q. To address this, we perform a singular value decomposition (SVD) and extract the leading component of the interpolated value, ensuring that $Q_0 \circ \Psi_{\Delta t} = q_{\Psi_{\Delta t}} \otimes q_{\Psi_{\Delta t}}$, and thereby $Q_{\Delta t}$ remains of rank 1. Finally, by projecting $Q_{\Delta t}$ on to the surface using tangent bases, we recover the intrinsic representation of $Q_{\Delta t}$ and its corresponding complex representation $[q]_{\Delta t} = \mathcal{V}^{-1}(Q_{\Delta t})$.

To model the Jeffery equation $\dot{Q} + \mathcal{P}^E(\mathcal{L}_u^\lambda Q) = 0$ (cf. equation (2.28)), we can include the additional rotational Lie advection $\mathcal{L}_u^{\text{rot}}$ and normalization as follows:

$$Q_{\Delta t} = \frac{\lambda F^{-1}(Q_0 \circ \Psi_{\Delta t}) F^{-\top} + (1-\lambda) R^{-1}(Q_0 \circ \Psi_{\Delta t}) R^{-\top}}{|\lambda F^{-1}(Q_0 \circ \Psi_{\Delta t}) F^{-\top} + (1-\lambda) R^{-1}(Q_0 \circ \Psi_{\Delta t}) R^{-\top}|}, \tag{3.5}$$

where R isolates rotation in F through polar decomposition $F = RU$. By omitting the normalization step and adjusting the value of λ, we can adapt the Jeffery advection to other commonly used convective rates, including the standard Lie derivative ($\lambda = 1$) and the Jaumann corotational derivative ($\lambda = 0$).

As a side remark, in the special case where the transported field h is a scalar function, its advection $\partial_t h + \mathcal{L}_u h = \partial_t h + \nabla_u h = 0$ simplifies to the traditional sL method, $h_{\Delta t} = \Psi_{\Delta t}^* h_0 = h_0 \circ \Psi_{\Delta t}$.

(iii) Discussion of sL advection scheme

Although the traditional scalar sL method guarantees unconditional stability, the extension to tensor Lie advection in general does not [28]. In these cases, stability depends on the pullback map's conditioning, requiring a Courant–Friedrichs–Lewy (CFL)-like condition to be met. However, by incorporating a diffusion term into the sL advection through time-splitting (cf. algorithm 1) and scaling the system with respect to advection, the time step for advection remains fixed regardless of the Péclet number. Because the diffusion equation, $\dot{[q]} = Pe^{-1} \Delta^L [q]$, is solved using an implicit method (cf. algorithm 1), the algorithm is numerically stable with high Pe. However, as Pe increases, maintaining accuracy requires resolving smaller physical length scales (which scale with $\sqrt{1/Pe}$), which in turn necessitates smaller time steps to satisfy the CFL condition.

We also acknowledge some known limitations inherent to time-splitting and the sL method. First, time-spliting introduces errors, which can be reduced using techniques such as the

Algorithm 2. sL method for nematic Lie advection over time interval $[0, \Delta t]$.

Inputs:
Surface mesh M, nematic field $Q_0 = \mathcal{V}([q]_0)$, time step Δt, flow velocity $\boldsymbol{u}$
for each vertex $v \in \mathfrak{V}$, **do**
  $\Psi_{\Delta t} \leftarrow \mathrm{RK4}(d\Psi_\tau/d\tau = -\boldsymbol{u}(\Psi_\tau))$ ▷ Backward flowmap
  $Q_{\Psi_{\Delta t}} \leftarrow \textsc{Interp}(Q_0 \circ \Psi_{\Delta t})$
  $Q_{\Psi_{\Delta t}} \leftarrow \mathrm{SVD}(Q_{\Psi_{\Delta t}})$
end for
for each face $f \in \mathfrak{F}$ **do** ▷ Deformation gradient
  $d\Psi_{\Delta t} \leftarrow [\boldsymbol{l}_1, \boldsymbol{l}_2, \boldsymbol{n}]_{\Psi_{\Delta t}}[\boldsymbol{l}_1, \boldsymbol{l}_2, \boldsymbol{n}]^{-1}$
end for
for each vertex $v \in \mathfrak{V}$, **do** ▷ Pullback
  $\boldsymbol{F} \leftarrow \textsc{Avg}(d\Psi_{\Delta t}|_{f \succ v})$
  $Q_v \leftarrow \boldsymbol{F}^{-1} Q_{\Psi_{\Delta t}} \boldsymbol{F}^{-\top}$
end for

Strang method [81]. Second, the sL method based on linear interpolation has significant numerical diffusion. Improvements can be made by implementing higher-order interpolation and techniques such as the McCormack scheme [81]. However, these challenges are common to the sL method and are not unique to the generalization to tensor-valued functions. Despite these challenges, the current minimal implementation is sufficient for our purpose of studying active nematics on curved surfaces.

(c) Gradient and covariant divergence

We used the linear finite-element hat function Φ_v to discretize the gradient for a scalar function $p \in C_{\mathfrak{V}}(M)$ as follows:

$$\mathrm{grad} : C_{\mathfrak{V}}(M) \to \Gamma_{\mathfrak{F}}(TM), \quad A_f(\mathrm{grad}\, p)_f = A_f \sum_{v \prec f} p_v(\mathrm{grad}_f \Phi_v) = \frac{1}{2} \sum_{v \prec f} p_v \mathbf{i}\boldsymbol{l}_{v \prec f}, \tag{3.6}$$

where $\mathbf{i}\boldsymbol{l}_{v \prec f}$ denotes the 90° rotation of edge vector $\boldsymbol{l}_{v \prec f}$ and A_f is the face area (cf. electronic supplementary material, S3 for mesh notation details).

The divergence operator is given by the negated adjoint operation of the gradient. The adjoint of equation (3.6) applied to a face-based vector field $\boldsymbol{u} \in \Gamma_{\mathfrak{F}}(TM)$ is a measure on each vertex $(\mathrm{grad}^* \boldsymbol{u})_v = -\frac{1}{2} \sum_{f \succ v} \langle \mathbf{i}\boldsymbol{l}_{v \prec f}, \boldsymbol{u}_f \rangle$, representing the total divergence at vertex v. Using a reference vertex area measure A_v, we define the divergence operator as

$$\mathrm{div} : \Gamma_{\mathfrak{F}}(TM) \to C_{\mathfrak{V}}(M), \quad A_v(\mathrm{div}\, \boldsymbol{u})_v = -\frac{1}{2} \sum_{f \succ v} \langle \mathbf{i}\boldsymbol{l}_{v \prec f}, \boldsymbol{u}_f \rangle. \tag{3.7}$$

Note that the discrete equation involving the divergence operator is often written in the weak form, where divergence is treated as a measure. In particular these discrete equations are independent of the specific choice of the vertex area measure A_v. In cases where pointwise evaluation is needed, such as in visualization, we use $A_v = \sum_{f \succ v} A_f/3$.

The divergence operator, represented by equation (3.7), can also be understood as a finite-volume discretization applied to the dual cells of the mesh [81]. We can analogously obtain a vertex-based divergence $\mathrm{div} : \Gamma_{\mathfrak{V}}(TM) \to C_{\mathfrak{F}}(M)$ by applying finite volume on the primal mesh.

By incorporating an additional vertex–face parallel transport, $\Pi_{v \rightsquigarrow f} : T_v M \to T_f M$, (cf. §3a(i)), we can extend such construction to discretize the covariant divergence

$$\mathrm{div}^\nabla : \Gamma_{\mathfrak{V}}(TM \otimes TM) \to \Gamma_{\mathfrak{F}}(TM), \quad A_f(\mathrm{div}^\nabla \boldsymbol{Q})_f = -\frac{1}{2} \sum_{v \prec f} \Pi_{v \rightsquigarrow f}[\boldsymbol{Q}_v \cdot \Pi^{-1}_{v \rightsquigarrow f}(\mathbf{i}\boldsymbol{l}_{v \prec f})]. \tag{3.8}$$

The Euclidean dot product, denoted as $\cdot$, denotes a contraction operation on one slot of the $(2,0)$ tensor (i.e. $\boldsymbol{Q}\cdot\boldsymbol{q}\equiv Q^{ij}q_j$). In the case of $\boldsymbol{Q}=\boldsymbol{q}\otimes\boldsymbol{q}$ being rank-1, the covariant divergence can be explicitly expressed, $A_f(\mathrm{div}^{\nabla}\boldsymbol{Q})_f=-(1/2)\sum_{v\prec f}\langle \Pi_{v\rightsquigarrow f}(\boldsymbol{q}_v),\mathbf{i}\boldsymbol{l}_{v\prec f}\rangle\Pi_{v\rightsquigarrow f}(\boldsymbol{q}_v)$. In practice, these discrete operators, including those in §3d, are organized and computed using sparse matrix multiplication.

(d) Bochner Laplacian

Using the face–face parallel transport $\Pi_{i\rightsquigarrow j}, i,j\in\mathfrak{F}$ across edge $e\prec i,j$ (cf. equation (3.1)), the discrete directional covariant derivative ∇_{l^*} maps a face-based vector field $\boldsymbol{u}=\hat{u}\mathbf{1}\in\Gamma_{\mathfrak{F}}(TM)$ to an edge-based vector field,

$$\nabla_{l^*}:\Gamma_{\mathfrak{F}}(TM)\to\Gamma_{\mathfrak{E}}(TM),\quad |\boldsymbol{l}_e^*|(\nabla_{l^*}\boldsymbol{u})_e=(\boldsymbol{u}_j-\Pi_{i\rightsquigarrow j}(\boldsymbol{u}_i))_{i,j\succ e}=((\hat{u}_j-e^{-\mathbf{i}\Omega_{e^*}}\hat{u}_i)\mathbf{1}_j)_{i,j\succ e}. \tag{3.9}$$

By taking the L_2 norm with the edge area as the diamond area formed by $\boldsymbol{l}$ and $\boldsymbol{l}^*$, $A_e=|\boldsymbol{l}||\boldsymbol{l}^*|$, we can construct the discrete Dirichlet energy (cf. equation (2.12)) as

$$2\mathcal{F}(\boldsymbol{u})=\sum_{e\in\mathfrak{E}}A_e|\nabla_{l^*}\boldsymbol{u}|_e^2=\sum_{e\in\mathfrak{E}}\frac{A_e}{|\boldsymbol{l}_e^*|^2}|\boldsymbol{u}_j-\Pi_{i\rightsquigarrow j}(\boldsymbol{u}_i)|_{i,j\succ e}^2=\sum_{e\in\mathfrak{E}}\frac{1}{w_e}|\hat{u}_j-e^{-\mathbf{i}\Omega_{e^*}}\hat{u}_i|_{i,j\succ e}^2. \tag{3.10}$$

The edge length ratio $w_e=|\boldsymbol{l}^*|/|\boldsymbol{l}|=(\cot\angle_{e\prec i}+\cot\angle_{e\prec j})/2$ is commonly referred to as the cotangent weight, where $\angle_{e\prec i}$ refers to the corner angle opposite to the edge e at face i.

The discrete Bochner Laplacian can be obtained by taking the negated variation of the discrete Dirichlet energy,

$$\Delta:\Gamma_{\mathfrak{F}}(TM)\to\Gamma_{\mathfrak{F}}(TM),\quad A_f(\Delta\boldsymbol{u})_f=-\left(\frac{\delta\mathcal{E}}{\delta\boldsymbol{u}}\right)_f=-\mathbf{1}_f\sum_{e\prec f}\frac{1}{w_e}(\hat{u}_f-e^{-\mathbf{i}\Omega_{e^*}}\hat{u}_i)_{i,f\succ e}. \tag{3.11}$$

Here, face i is in the one-ring neighbour of face f, and i and f share the edge e.

Similarly, using the vertex–vertex transportation $\Pi_{i\rightsquigarrow j}, i,j\in\mathfrak{V}$ across edge $e\succ i,j$ (cf. equation (3.2)), we can construct the covariant derivative for a vertex-based nematic field as follows:

$$\nabla_l^L:\Gamma_{\mathfrak{V}}(TM)\to\Gamma_{\mathfrak{E}}(TM),\quad |\boldsymbol{l}_e|(\nabla_l[\boldsymbol{q}])_e=([\boldsymbol{q}]_j-\Pi_{i\rightsquigarrow j}([\boldsymbol{q}]_i))_{i,j\prec e}=((\hat{q}_j-e^{-\mathbf{i}2\Omega_e}\hat{q}_i)[\mathbf{1}]_j)_{i,j\prec e}. \tag{3.12}$$

The nematic Bochner Laplacian acting on the vertex-based nematic field $[\boldsymbol{q}]=[\hat{q}][\mathbf{1}]\in\Gamma_{\mathfrak{V}}(L)$ is therefore

$$\Delta^L:\Gamma_{\mathfrak{V}}(L)\to\Gamma_{\mathfrak{V}}(L),\quad A_v(\Delta[\boldsymbol{q}])_v=-[\mathbf{1}]_v\sum_{e\prec v}w_e([\hat{q}]_v-e^{-\mathbf{i}2\Omega_e}[\hat{q}]_i)_{i,f\prec e}, \tag{3.13}$$

where vertex i is in the one-ring neighbour of vertex v, connected by edge e.

Strictly speaking, there is an ambiguity in the definition of the directional covariant derivative (equations (3.9) and (3.12)) because it is equally valid to transport a vector (nematic director) from face (vertex) j to face (vertex) i before applying finite difference. However, the discretization of the Dirichlet energy, and thus the Bochner Laplacian (equations (3.11) and (3.13)), relies only on the norm of the covariant derivative, which remains invariant, $|\Pi_{j\rightsquigarrow i}(\boldsymbol{u}_j)-\boldsymbol{u}_i|=|\boldsymbol{u}_j-\Pi_{i\rightsquigarrow j}(\boldsymbol{u}_i)|$, $|\Pi_{j\rightsquigarrow i}([\boldsymbol{q}]_j)-[\boldsymbol{q}]_i|=|[\boldsymbol{q}]_j-\Pi_{i\rightsquigarrow j}([\boldsymbol{q}]_i)|$.

In summary, the intrinsic definition of the discrete Bochner Laplacian emerges naturally from continuous theory of complex line bundles. Contrasting the previous covariant divergence (equation (3.8)) that relies on an extrinsic parallel transport achieved through dihedral rotations between the tangent spaces of vertices and faces, the Bochner Laplacian is constructed purely intrinsically by vertex–vertex or face–face parallel transport. Compared with common approaches that rely on the embedding structure in $\mathbb{R}^3$ and a projection operator from $\mathbb{R}^3$ to the manifold, the discrete complex line bundle approach has notably improved efficiency. This approach reduces the degree of freedom per element from 3 to 2, and the complex nature furthermore takes advantage of the optimized complex arithmetic handling in established numerical linear algebra libraries. The corresponding complex-valued Laplace matrix is Hermitian and negative-semidefinite.

(e) Curvature, defects and local-global geometry

Here, we introduce a discretization of the face Gaussian curvature and an algorithm to detect topological defects and compute their charges. This serves as the discrete counterpart to the continuous theory in §2a(vii).

Given a vertex-based k-atic field $[\boldsymbol{q}]_k : \mathfrak{V} \to V_k$, we can use vertex–vertex parallel transport $\Pi_{i\to j}$ (cf. equation (3.2)) with $i, j \in \mathfrak{V}$ along the incident edge $e \succ i, j$ to measure the finite rotation $|\boldsymbol{l}_e|\eta_e$ (cf. equation (2.16)) of $[\boldsymbol{q}]_k$ along e as follows:

$$|\boldsymbol{l}_e|\eta_e = \arg\left(\frac{[\boldsymbol{q}]_{k,j}}{\Pi_{i\rightsquigarrow j}[\boldsymbol{q}]_{k,i}}\right) = \arg\left(\frac{[\hat{\boldsymbol{q}}]_{k,j}}{e^{-\mathrm{i}k\Omega_e}[\hat{\boldsymbol{q}}]_{k,i}}\right). \tag{3.14}$$

Assuming the k-atic field $[\boldsymbol{q}]_k$ is continuous between vertices i and j, we choose the principal branch of the arg function so that $|\boldsymbol{l}_e|\eta_e$ lies within $(-\pi, \pi]$.

Recall that in the continuous setting, Gaussian curvature quantifies holonomy, $\int_U K dA = -\int_{\partial U} \omega$ (cf. §2a(vii)). Analogously, discrete Gaussian curvature $K \in C_{\mathfrak{F}}(M)$ can be represented by closed-loop summation of the primal edge connection Ω_e as

$$A_f K_f := -\sum_{e\prec f} \Omega_e \mod 2\pi \in (-\pi, \pi]. \tag{3.15}$$

Selecting branch $(-\pi, \pi]$ for $A_f K_f$ is justified by the small integration domain of face f. The discrete curvature is also the angle defect at face f, given by $A_f K_f = \sum_{v\prec f} \tilde{\angle}_v - \pi$, where $\tilde{\angle}_v$ is the geodesic corner angle (cf. electronic supplementary material, S3). The discrete Gauss–Bonnet theorem states, $\sum_f A_f K_f = 2\pi\chi(M)$, where $\chi(M) = |\mathfrak{V}| - |\mathfrak{E}| + |\mathfrak{F}| = 2 - 2g$ represents the Euler characteristic of the polygonal mesh M.

Analogous to equation (2.17) in the continuous theory, given a k-atic field $[\boldsymbol{q}]_k$, its topological charge is a fraction-valued function $\mathcal{Z}([\boldsymbol{q}]_k) : \mathfrak{F} \to \mathbb{Z}/k$ that can be computed for each face f as follows:

$$\mathcal{Z}_f([\boldsymbol{q}]_k) = \frac{1}{2\pi k}\sum_{e\prec f} |\boldsymbol{l}_e|\eta_e + \frac{1}{2\pi} A_f K_f. \tag{3.16}$$

The charge $\mathcal{Z}_f$ at face f is zero when the adjacent k-atic directors $[\boldsymbol{q}]_{k,v\prec f}$ are continuous, and non-zero in the presence of defects. The charge function satisfies the discrete Poincaré–Hopf theorem exactly, $\sum_f \mathcal{Z}_f([\boldsymbol{q}]_k) = \chi(M)$.

(f) AL method for the Stokes equations

We use a classic AL iteration to solve the incompressible Stokes flow [82]. Recall that the Stokes equations can be viewed as the stationary condition for a divergence-constrained variational problem (cf. §2b(i)). The AL approach augments the original Rayleighian with a quadratic penalty term on the divergence. The augmented Rayleighian is given by

$$\min_{\boldsymbol{u}} \max_{p} \ \mathcal{R}_{\mathrm{AL}} = \mathcal{R}(\boldsymbol{u}, p) + \frac{k}{2}\langle\!\langle \operatorname{div} \boldsymbol{u}, \operatorname{div} \boldsymbol{u}\rangle\!\rangle, \tag{3.17}$$

where the stationary condition is $(\Delta + K + k\,\mathrm{grad} \circ \mathrm{div})\boldsymbol{u} - \mathrm{grad}\, p + \boldsymbol{f} = 0$. Here, the penalty coefficient k enforces the incompressibility constraint during the iterative solution process. Shown in algorithm 3, the solve process involves iteratively solving the modified Stokes equations. At each iteration, the velocity and pressure fields are updated until a convergence criterion is met. Practically, increasing k makes the fluid very stiff in response to compressibility, which leads to convergence in a small number of iterations. However, a high value of k also increases the spectral condition number of $(\Delta + K + k\,\mathrm{grad} \circ \mathrm{div})$, which increases the time per iteration [82].

As discussed in §2b(i), when dealing with the Stokes equations in symmetric geometries that possess a Killing vector field, the solution is not unique. To ensure that we obtain continuous solution during time evolution, we consistently select the solution with the minimal L_2 norm by

Algorithm 3. AL subroutine for incompressible Stokes equations.

Inputs:
  Penalty coefficient k, tolerance ε
Initialize:
  Initial guess p
while $\|\mathrm{div}\,\boldsymbol{u}\| > \varepsilon$ **do**
  $\boldsymbol{u} \leftarrow \textsc{Solve}(-(\Delta + K + k\,\mathrm{grad} \circ \mathrm{div})\boldsymbol{u} = \boldsymbol{f} - \mathrm{grad}\,p)$ ▷ Poisson solve (A x = b)
  $p \leftarrow p + k\,\mathrm{div}\,\boldsymbol{u}$
end while

if exist N distinct $\boldsymbol{\omega}_i$ **then** ▷ Remove the Killing component
  for $i = 1$ to N **do**
    $\boldsymbol{u} \leftarrow \boldsymbol{u} - \langle\langle \boldsymbol{u}, \boldsymbol{\omega}_i \rangle\rangle \boldsymbol{\omega}_i$
  end for
end if

projecting out components that lie in the space of the Killing vector fields. To achieve this, we precompute the set of Killing bases of the geometry, denoted as $\boldsymbol{\omega}_i$, before we begin the evolution of the active nematic system. The bases are determined by solving the non-vanishing vector field that satisfies $(\Delta + K + \mathrm{grad} \circ \mathrm{div})\boldsymbol{\omega}_i = 0$. In practice, we solve this equation computationally through the smallest eigenvalue problem and extract eigenfunctions with near-zero eigenvalues. Here, each Killing basis is normalized such that $\langle\langle \boldsymbol{\omega}_i, \boldsymbol{\omega}_j \rangle\rangle = \delta_{ij}$. As outlined in algorithm 3, we project out components spanned by these bases after the AL iteration. This protocol is carried out in §4 for examples on the sphere and torus.

4. Results and discussion

In this section, we demonstrate the robustness of our method and its potential in addressing various biophysically relevant scenarios. In electronic supplementary material, S4, we validate these methods through resolution studies on simple geometries, combining numerical experiments with analytical comparisons. We examine the Stokes equations, sL nematic advection and curvature estimation. Notably, we compare the numerical solution of surface Stokes flow against an analytical solution on a sphere using spherical harmonics. We also demonstrate the convergence properties of the AL method for imposing incompressibility in the Stokes equations. Performance and time complexity analyses, as well as the hardware used for the simulations, are detailed in electronic supplementary material, S5.

The application of our method extends beyond idealized geometries. To demonstrate its generality on arbitrary geometries and topologies, we apply it to solve the full nematodynamics equations in biophysically relevant examples. We initialize the system with a smooth nematic field by calculating the eigenmodes of the nematic Laplacian $\Delta^L[\boldsymbol{q}] = \lambda[\boldsymbol{q}]$ corresponding to eigenvalues λ close to zero. These eigenmodes approximate minimizers of the Frank–Oseen energy. The numerical experiments encompass analytical shapes such as spheres and genus-1 tori, and organic shapes characterized by arbitrary curvature distributions. As previously mentioned in §§ 2b(i) and 3(f), the Stokes equations have Killing vector fields as their kernel. On spheres and tori where such a Killing vector field exists, we carry out projections to remove the Killing component and focus on a specialized solution with a minimal L_2 norm. We present each example under two distinct levels of activity, distinguished by disparate Péclet numbers ($Pe = 1$ and $Pe = 10^4$, both extensile). They showcase both regular solutions and solutions in the regime of active turbulence.

To characterize the nematodynamics, we focus on recording key metrics, including defect counts (of charge $\pm 1/2$), the charge-curvature energy $||d\chi||^2 := ||\Sigma_i 2\pi \mathcal{Z}_{p_i}\delta_{p_i} - K||^2_{\Delta^{-1}}$ (except on the sphere where curvature is uniform), flow velocity $||\boldsymbol{u}||^2$ and enstrophy $||\mathcal{K}\boldsymbol{u}||^2$. Here, χ

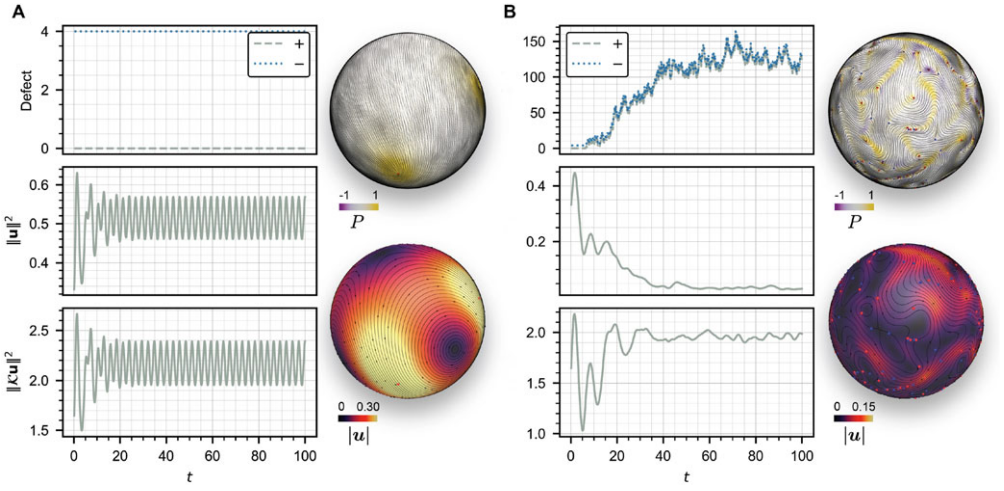

Figure 3. Nematodynamics on a sphere under two levels of activity, as captured by the Péclet number: (a) low activity ($Pe = 1$) and (b) high activity ($Pe = 10^4$). The animated time-series simulations are available on YouTube: https://youtu.be/gvihHbsWMsc. From top to bottom, the time plots show: the total numbers of $+1/2$ and $-1/2$ topological defects of the nematic field, the L_2 norm squared $||\boldsymbol{u}||^2$ of the fluid velocity and the enstrophy $||\mathcal{K}\boldsymbol{u}||^2$ of the surface flow. Snapshots of the system are captured at the conclusion of each set of simulations ($t = 100$). The upper snapshots display the nematic field, colour-mapped by the local power density exerted by the nematic on to the fluid, expressed as $P = -\langle \boldsymbol{u}, \mathrm{div}^{\nabla} \boldsymbol{Q} \rangle$. The lower snapshots visualize the velocity field, colour-mapped by its magnitude $|\boldsymbol{u}|$.

represents the *geometric potential* [41,83], defined by $\Delta\chi = 2\pi \mathcal{Z}_{p_i} \delta_{p_i} - K$ based on defect locations p_i and charges $\mathcal{Z}_{p_i}$ (cf. §2a(vii)), where δ_{p_i} denotes the Dirac delta function centred at p_i. The enstrophy quantifies viscous dissipation and serves to assess sharp features and chaotic behaviour. For each case at each Péclet number, we include visual snapshots captured at the end of the simulation. Taking figure 3 as an example, the top snapshot displays the texture of the nematic field, with positive defects shown in red and negative defects in blue. The bottom snapshot illustrates the streamlines of the fluid flow field, colour-mapped to represent velocity magnitude, $|\boldsymbol{u}|$. The colourmap on the nematic field represents the local power density exerted by the active nematic on the fluid, given by $P = -\langle \boldsymbol{u}, \mathrm{div}^{\nabla} \boldsymbol{Q} \rangle$. This expression captures the contribution of the active stress tensor to the fluid flow. Each positive half defect is accompanied by a self-propelling fluid jet and a vortex pair, and is surrounded by a region of positive power P. By contrast, negative half defects exhibit 3-atic symmetry and generate an index-2 flow field that is self-counteracting and remains static [84], contributing little energy to the fluid on large scales.

In figure 3a, we examine dynamics on a sphere at Péclet number $Pe = 1$, corresponding to a low activity level. Here, we observe a fixed number of four $+1/2$ defects exhibiting periodic orbiting motions—a phenomenon supported by previous empirical studies and simulations [3,11]. In figure 3b, we increase the activity level to $Pe = 10^4$, leading to the emergence of active turbulence. Active turbulence is characterized by unsteady and chaotic dynamics driven by the spontaneous formation and annihilation of topological defect pairs. Demonstrated by figure 3b and consistent with the existing literature [85], the onset of turbulence is characterized by the appearance of large bending deformation walls that separate aligned nematic regions, the creation and annihilation of nematic defect pairs, and the separation of positive defects from negative defects due to self-propulsion of the positive. As the total number of topological defects increases, intricate flow patterns develop at smaller length scales. This observation is supported by the fluctuating but steady enstrophy and a rapid decrease in the overall velocity magnitude in the time-series plots.

As our method is able to accommodate different topologies, we expand our exploration of nematodynamics to a genus-1 torus, characterized by a zero Euler characteristic. The vanishing

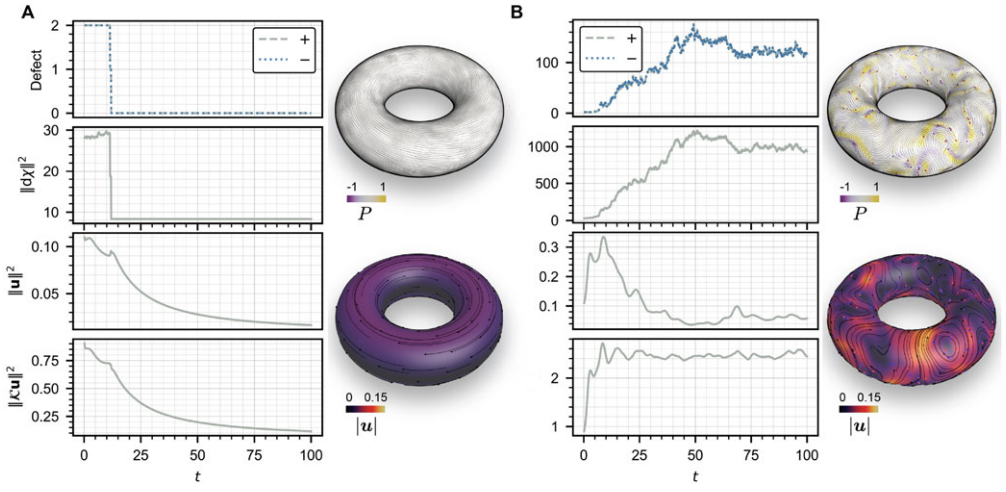

Figure 4. Nematodynamics on a torus at (a) $Pe = 1$ and (b) $Pe = 10^4$. The animated time-series simulations are available on YouTube: https://youtu.be/p4NLpHRTkPg. The energy $||d\chi||^2$ measures the charge-curvature correlation. Refer to figure 3 for detailed descriptions of the other elements in the figure.

Euler characteristic allows for a defect-free configuration at lower activity levels, as the nematic relaxation gradually merges two pairs of positive and negative defects (cf. figure 4a). A key observation is that the equilibrium defect-free nematic field on the torus displays rotational symmetry around its vertical axis, while maintaining a constant angle with the lines of toroidal coordinates. Consequently, the resulting Stokes flow also exhibits this rotational symmetry, with the toroidal midline acting as a shear layer. This flow pattern, in conjunction with diffusion, stabilizes the nematic field, allowing the system to reach a steady state. In figure 4b, when the Péclet number increases, the system transitions into a state of active turbulence through the injection of energy by topological defects, similar to what occurs on a sphere. Once again, we note that enstropy reaches a plateau soon after the initial defect proliferation, while the velocity norm decreases as vortices form on increasingly smaller length scales. The charge-curvature energy rises with the number of defects.

In addition to standard analytical shapes, we applied our method to a topologically spherical membrane structure with an arbitrary curvature distribution (cf. figure 5a). This geometry is generated through a simulation based on the Helfrich bending energy under the influence of an osmotic shock [86]. Even under low-activity conditions where nematic ordering relaxation prevails, a relatively large total number of defects persists. At the initial drop in $||d\chi||^2$ (cf. figure 5a and its animated movie), defects unbind and cluster in regions with like-sign curvature: positive defects gather at protrusions with positive curvature, while negative defects accumulate in negatively curved valleys (cf. electronic supplementary material, fig. S4). This behaviour aligns with equilibrium theories of liquid crystals [83]. When two positive defects are present at a protrusion, they create strong circulating flows at the tips. These flows cause the defects to orbit periodically around the protrusions. This interaction at the protrusion is isolated from the rest of the domain, which remains almost motionless, thereby creating a limit cycle in the system. The distinct behaviours of active nematics in areas of positive and negative curvature suggests a possible detailed comparative study on active nematic systems in hyperbolic and elliptic geometries as a follow-up work. More broadly, the division of the flow field into areas of positive and negative curvature has implications for understanding how mixing and coherent structures are influenced by the shape of the domain. As *Pe* increases, nonlinear hydrodynamic effects disrupt the charge-curvature correlation (cf. electronic supplementary material, fig. S4), consistent with observations in [41]. In addition, there is a notable difference in flow velocities when comparing conditions on a complex-shaped object to the sphere case. On a sphere, the

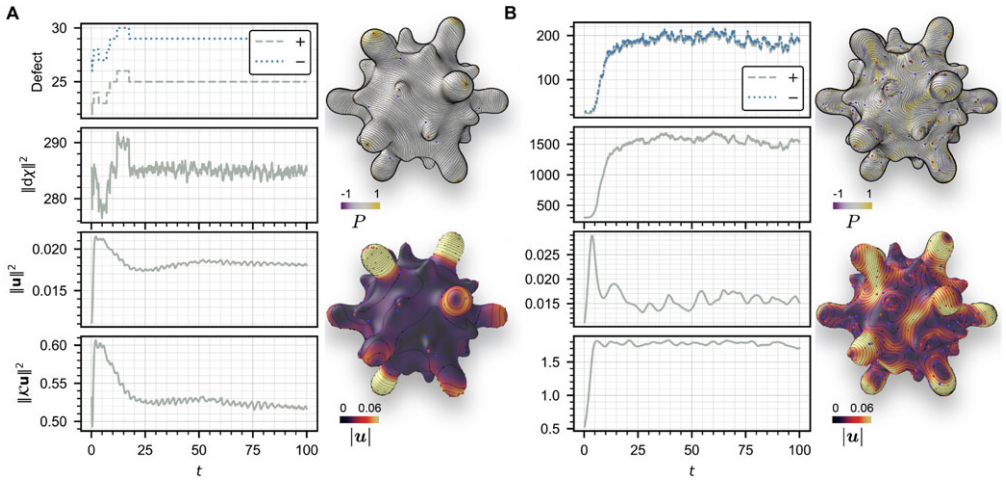

Figure 5. Nematodynamics on a topological sphere of varying curvature at (a) $Pe = 1$ and (b) $Pe = 10^4$. The animated time-series simulations are available on Youtube: https://youtu.be/hgsREDJwWZQ. The energy $||d\chi||^2$ measures the charge-curvature correlation. Refer to figure 3 for detailed descriptions of the other elements in the figure.

interaction of topological defects creates complex flow patterns on small length scales, which tends to reduce the characteristic magnitude of the fluid velocity. However, as seen in figure 5b, for the complex shape, the magnitude of velocities remains relatively consistent whether in a steady state at low *Pe* or in active turbulence at high *Pe*. Active turbulence breaks down the stable coherent flow structures at low *Pe*, leading to a state with more efficient mixing by the flow. Specifically, this results in a decrease in velocity at the protrusions and an increase in velocity in the valleys of the manifold.

5. Conclusion

In this study, we formulate a minimal model for the dynamics of an active nematic fluid on a Riemannian two-manifold. This model is cast based on a coordinate-free differential-geometric language and on the theory of the complex line bundle, which can naturally be generalized to curved spaces. We use the complex line to establish the two-dimensional *k*-atic equivalence and model nematic advection through generalized Lie derivatives, laying the groundwork for extending the model to *k*-atic hydrodynamics. The Levi–Civita connection and its curvature are introduced within the framework of the complex line bundle. We show the coupling of the fluid's viscous stress with the curvature through the covariant Dolbeault $\bar{\partial}^{\nabla}$ operator. Numerically, our method evolves the active nematic system on a triangular mesh with arbitrary shape and topology. This is done by adhering to the discrete analogue of the continuous theory. We construct the Hermitian Bochner Laplacian matrix based on the variational principle and develop a generalized sL scheme according to the Lie advection. This method maintains robustness and efficiency across various flow regimes, from low to high activity levels.

In future work, we anticipate detailed studies that examine the relationship between the complex number representation and the well-established $\boldsymbol{Q}$-tensor theory, including their generalizations to *k*-atic fields. While our theoretical framework is general, the current implementation is limited to closed manifolds; future work could incorporate boundary conditions. We acknowledge that our minimal Riemannian nematodynamics model does not account for reactive stresses due to nematic elasticity in advection [63], extrinsic geometry [76,77] or the out-of-plane component of the nematic field [78]. These aspects will be addressed in future research. Depending on the specific application, it may also be important to consider fluid equations on evolving surfaces [9,42,68,87,88] and their coupling with bulk fluid [3,89].

In summary, our integration of geometric language and complex manifold theory into the study of active nematics sets the stage for further theoretical and computational developments in this area. With further post-processing and analysis, we expect that the computational tool developed here will also be instrumental for specialists seeking deeper understanding of active nematics influenced by geometric aspects in specific systems. We hope that the incorporation of realistic geometric and topological features in the model can further narrow the gap between theoretical predictions and experimental findings.

Data accessibility. The code developed in this paper can be accessed at [90].

The data are provided in electronic supplementary material [91].

Declaration of AI use. We have not used AI-assisted technologies in creating this article.

Authors' contributions. C.Z.: conceptualization, data curation, formal analysis, investigation, methodology, software, validation, visualization, writing—original draft; D.S.: conceptualization, funding acquisition, investigation, methodology, project administration, resources, supervision, writing—review and editing; A.C.: conceptualization, funding acquisition, investigation, methodology, project administration, resources, supervision, writing—review and editing.

All authors gave final approval for publication and agreed to be held accountable for the work performed therein.

Conflict of interest declaration. We declare we have no competing interests.

Funding. D.S. acknowledges funding from National Science Foundation grant no. DMS-2153520. A.C. acknowledges funding from National Science Foundation CAREER Award 2239062. Additional support was provided by SideFX software.

Acknowledgements. C.Z. thanks M. Firouznia and Y. Chen for their helpful references and many discussions on various topics covered in this study.

References

1. Alert R, Casademunt J, Joanny JF. 2022 Active turbulence. *Annu. Rev. Condens. Matter Phys.* **13**, 143–170. (doi:10.1146/annurev-conmatphys-082321-035957)
2. Doostmohammadi A, Ignés-Mullol J, Yeomans JM, Sagués F. 2018 Active nematics. *Nat. Commun.* **9**, 3246. (doi:10.1038/s41467-018-05666-8)
3. Firouznia M, Saintillan D. 2025 Self-organized dynamics of a viscous drop with interfacial nematic activity. *Phys. Rev. Res.* **7**, L012054. (doi:10.1103/PhysRevResearch.7.L012054)
4. Apaza L, Sandoval M. 2018 Active matter on Riemannian manifolds. *Soft Matter* **14**, 9928–9936. (doi:10.1039/C8SM01034J)
5. Mietke A, Jülicher F, Sbalzarini IF. 2019 Self-organized shape dynamics of active surfaces. *Proc. Natl Acad. Sci. USA* **116**, 29–34. (doi:10.1073/pnas.1810896115)
6. Hoffmann LA, Carenza LN, Eckert J, Giomi L. 2022 Theory of defect-mediated morphogenesis. *Sci. Adv.* **8**, eabk2712. (doi:10.1126/sciadv.abk2712)
7. Bell S, Lin SZ, Rupprecht JF, Prost J. 2022 Active nematic flows over curved surfaces. *Phys. Rev. Lett.* **129**, 118001. (doi:10.1103/PhysRevLett.129.118001)
8. Al-Izzi SC, Morris RG. 2021 Active flows and deformable surfaces in development. *Seminars Cell Dev. Biol.* **120**, 44–52. (doi:10.1016/j.semcdb.2021.07.001)
9. Al-Izzi SC, Morris RG. 2023 Morphodynamics of active nematic fluid surfaces. *J. Fluid Mech.* **957**, A4. (doi:10.1017/jfm.2023.18)
10. Zhang R, Zhou Y, Rahimi M, De Pablo JJ. 2016 Dynamic structure of active nematic shells. *Nat. Commun.* **7**, 13483. (doi:10.1038/ncomms13483)
11. Keber FC, Loiseau E, Sanchez T, DeCamp SJ, Giomi L, Bowick MJ, Marchetti MC, Dogic Z, Bausch AR. 2014 Topology and dynamics of active nematic vesicles. *Science* **345**, 1135–1139. (doi:10.1126/science.1254784)
12. Napoli G, Vergori L. 2012 Extrinsic curvature effects on nematic shells. *Phys. Rev. Lett.* **108**, 207803. (doi:10.1103/PhysRevLett.108.207803)
13. Napoli G, Vergori L. 2016 Hydrodynamic theory for nematic shells: the interplay among curvature, flow, and alignment. *Phys. Rev. E* **94**, 020701. (doi:10.1103/PhysRevE.94.020701)
14. Giomi L, Toner J, Sarkar N. 2022 Hydrodynamic theory of p-atic liquid crystals. *Phys. Rev. E* **106**, 024701. (doi:10.1103/PhysRevE.106.024701)

15. Vafa F, Zhang GH, Nelson DR. 2022 Defect absorption and emission for *p*-atic liquid crystals on cones. *Phys. Rev. E* **106**, 024704. (doi:10.1103/PhysRevE.106.024704)
16. Vafa F. 2022 Defect dynamics in active polar fluids vs. active nematics. *Soft Matter* **18**, 8087–8097. (doi:10.1039/D2SM00830K)
17. Sonnet AM, Virga EG. 2012 *Dissipative ordered fluids: theories for liquid crystals*. New York, NY, USA: Springer Science & Business Media.
18. Salbreux G, Prost J, Joanny JF. 2009 Hydrodynamics of cellular cortical flows and the formation of contractile rings. *Phys. Rev. Lett.* **103**, 058102. (doi:10.1103/PhysRevLett.103.058102)
19. Kaiser P, Wiese W, Hess S. 1992 Stability and instability of an uniaxial alignment against biaxial distortions in the isotropic and nematic phases of liquid crystals. *J. Non-Equilib. Thermodyn.* **17**, 153–169. (doi:10.1515/jnet.1992.17.2.153)
20. Bhattacharjee A, Menon GI, Adhikari R. 2008 Numerical method of lines for the relaxational dynamics of nematic liquid crystals. *Phys. Rev. E* **78**, 026707. (doi:10.1103/PhysRevE.78.026707)
21. Doi M, Edwards SF. 1988 *The theory of polymer dynamics*. Oxford, UK: Clarendon Press.
22. Bird RB, Hassager O, Armstrong RC, Curtiss CF. 1988 *Dynamics of polymeric liquids: kinetic theory*. New York, NY: Wiley Intersciencem.
23. Beris AN, Edwards BJ. 1994 *Thermodynamics of flowing systems with internal microstructure*. Oxford, UK: Oxford University Press.
24. Saintillan D, Shelley MJ. 2013 Active suspensions and their nonlinear models. *C.R. Phys.* **14**, 497–517. (doi:10.1016/j.crhy.2013.04.001)
25. Morozov A, Spagnolie SE. 2015 Introduction to complex fluids. In *Complex fluids in biological systems: experiment, theory, and computation* (ed. SE Spagnolie), pp. 3–52. New York, NY: Springer.
26. Gilbert AD, Vanneste J. 2023 A geometric look at momentum flux and stress in fluid mechanics. *J. Nonlinear Sci.* **33**, 31. (doi:10.1007/s00332-023-09887-0)
27. Wensch J, Naumann A. 2012 Semi-Lagrangian discretization of the upper-convective derivative in non-Newtonian fluid flow. *Proc. Appl. Math. Mech.* **12**, 765–766. (doi:10.1002/pamm.201210371)
28. Nabizadeh MS, Wang S, Ramamoorthi R, Chern A. 2022 Covector fluids. *ACM Trans. Graph.* **41**, 1–16. (doi:10.1145/3528223.3530120)
29. Mullen P, McKenzie A, Pavlov D, Durant L, Tong Y, Kanso E, Marsden JE, Desbrun M. 2011 Discrete lie advection of differential forms. *Found. Comput. Math.* **11**, 131–149. (doi:10.1007/s10208-010-9076-y)
30. Pismen LM. 1999 *Vortices in nonlinear fields: from liquid crystals to superfluids, from non-equilibrium patterns to cosmic strings*. Oxford, UK: Oxford University Press.
31. Chan CH, Czubak M, Disconzi MM. 2017 The formulation of the Navier–Stokes equations on Riemannian manifolds. *J. Geometry Phys.* **121**, 335. (doi:10.1016/j.geomphys.2017.07.015)
32. Samavaki M, Tuomela J. 2020 Navier–Stokes equations on Riemannian manifolds. *J. Geometry Phys.* **148**, 103543. (doi:10.1016/j.geomphys.2019.103543)
33. Nestler M, Voigt A. 2022 Active nematodynamics on curved surfaces–the influence of geometric forces on motion patterns of topological defects. *Commun. Comput. Phys.* **31**, 947–965. (doi:10.4208/cicp.OA-2021-0206)
34. Rank M, Voigt A. 2021 Active flows on curved surfaces. *Phys. Fluids* **33**, 072110. (doi:10.1063/5.0056099)
35. Brandner P, Jankuhn T, Praetorius S, Reusken A, Voigt A. 2022 Finite element discretization methods for velocity-pressure and stream function formulations of surface Stokes equations. *SIAM J. Sci. Comput.* **44**, A1807. (doi:10.1137/21M1403126)
36. Reuther S, Nitschke I, Voigt A. 2020 A numerical approach for fluid deformable surfaces. *J. Fluid Mech.* **900**, R8. (doi:10.1017/jfm.2020.564)
37. Zhang R, Roberts T, Aranson IS, De Pablo JJ. 2016 Lattice Boltzmann simulation of asymmetric flow in nematic liquid crystals with finite anchoring. *J. Chem. Phys.* **144**, 084905. (doi:10.1063/1.4940342)
38. Nitschke I, Reuther S, Voigt A. 2021 Vorticity–stream function approaches are inappropriate to solve the surface Navier–Stokes equation on a torus. *Proc. Appl. Math. Mech.* **20**, e202000006. (doi:10.1002/pamm.202000006)

39. Yin H, Nabizadeh MS, Wu B, Wang S, Chern A. 2023 Fluid cohomology. *ACM Trans. Graph.* **42**, 126. (doi:10.1145/3592402)
40. Reusken A. 2020 Stream function formulation of surface Stokes equations. *IMA J. Numer. Anal.* **40**, 109. (doi:10.1093/imanum/dry062)
41. Pearce D, Ellis PW, Fernandez-Nieves A, Giomi L. 2019 Geometrical control of active turbulence in curved topographies. *Phys. Rev. Lett.* **122**, 168002. (doi:10.1103/PhysRevLett.122.168002)
42. Torres-Sánchez A, Millán D, Arroyo M. 2019 Modelling fluid deformable surfaces with an emphasis on biological interfaces. *J. Fluid Mech.* **872**, 218–271. (doi:10.1017/jfm.2019.341)
43. Gross S, Jankuhn T, Olshanskii MA, Reusken A. 2018 A trace finite element method for vector-Laplacians on surfaces. *SIAM J. Numer. Anal.* **56**, 2406–2429. (doi:10.1137/17M1146038)
44. Ben-Chen M, Butscher A, Solomon J, Guibas L. 2010 On discrete Killing vector fields and patterns on surfaces. *Comput. Graph. Forum* **29**, 1701–1711. (doi:10.1111/j.1467-8659.2010.01779.x)
45. de Goes F, Liu B, Budninskiy M, Tong Y, Desbrun M. 2014 Discrete 2-tensor fields on triangulations. *Comput. Graph. Forum* **33**, 13–24. (doi:10.1111/cgf.12427)
46. De Goes F, Butts A, Desbrun M. 2020 Discrete differential operators on polygonal meshes. *ACM Trans. Graph. (TOG)* **39**, 110–1. (doi:10.1145/3386569.3392389)
47. Knöppel F, Crane K, Pinkall U, Schröder P. 2013 Globally optimal direction fields. *ACM Trans. Graph.* **32**, 1–10. (doi:10.1145/2461912.2462005)
48. Sageman-Furnas AO, Chern A, Ben-Chen M, Vaxman A. 2019 Chebyshev nets from commuting PolyVector fields. *ACM Trans. Graph.* **38**, 1–16. (doi:10.1145/3355089.3356564)
49. De Goes F, Desbrun M, Tong Y. 2016 Vector field processing on triangle meshes. In *ACM SIGGRAPH 2016 Courses, Anaheim, California*, pp. 1–49. New York, NY, USA: Association for Computing Machinery. See https://doi.org/10.1145/2897826.2927303.
50. Jacobson N. 2012 *Basic algebra I*. New York, NY, USA: Dover Publications.
51. Marsden JE, Hughes TJ. 1994 *Mathematical foundations of elasticity*. New York, NY, USA: Dover Publications.
52. Schutz BF. 1980 *Geometrical methods of mathematical physics*. Cambridge, UK: Cambridge University Press.
53. Kanso E, Arroyo M, Tong Y, Yavari A, Marsden JG, Desbrun M. 2007 On the geometric character of stress in continuum mechanics. *Z. Angew. Math. Phys.* **58**, 843–856. (doi:10.1007/s00033-007-6141-8)
54. Oldroyd JG. 1950 On the formulation of rheological equations of state. *Proc. R. Soc. Lond. A* **200**, 523–541. (doi:10.1098/rspa.1950.0035)
55. Needham T. 2021 *Visual differential geometry and forms: a mathematical drama in five acts*. Princeton, NJ: Princeton University Press.
56. Needham T. 2023 *Visual complex analysis*. Oxford, UK: Oxford University Press.
57. Arroyo M, DeSimone A. 2009 Relaxation dynamics of fluid membranes. *Phys. Rev. E* **79**, 031915. (doi:10.1103/PhysRevE.79.031915)
58. Saffman PG, Delbrück M. 1975 Brownian motion in biological membranes.. *Proc. Natl Acad. Sci. USA* **72**, 3111–3113. (doi:10.1073/pnas.72.8.3111)
59. Doi M. 2013 *Soft matter physics*. Oxford, UK: Oxford University Press.
60. Doi M. 2011 Onsager's variational principle in soft matter. *J. Phys.: Condens. Matter* **23**, 284118. (doi:10.1088/0953-8984/23/28/284118)
61. Arroyo M, Walani N, Torres-Sánchez A, Kaurin D. 2018 Onsager's variational principle in soft matter: introduction and application to the dynamics of adsorption of proteins onto fluid membranes. In *The role of mechanics in the study of lipid bilayers* (ed. DJ Steigmann), pp. 287–332. New York, NY: Springer International Publishing.
62. Mirza W, Torres-Sánchez A, Vilanova G, Arroyo M. 2023 Variational formulation of active nematics: theory and simulation. (http://arxiv.org/abs/2306.01515)
63. Bouck L, Nochetto RH, Yushutin V. 2024 A hydrodynamical model of nematic liquid crystal films with a general state of orientational order. *J. Nonlinear Sci.* **34**, 5. (doi:10.1007/s00332-023-09970-6)
64. Saintillan D. 2018 Rheology of active fluids. *Annu. Rev. Fluid Mech.* **50**, 563–592. (doi:10.1146/annurev-fluid-010816-060049)
65. Thampi SP, Doostmohammadi A, Golestanian R, Yeomans JM. 2015 Intrinsic free energy in active nematics. *Europhys. Lett.* **112**, 28004. (doi:10.1209/0295-5075/112/28004)

66. Gao T, Betterton MD, Jhang AS, Shelley MJ. 2017 Analytical structure, dynamics, and coarse graining of a kinetic model of an active fluid. *Phys. Rev. Fluids* **2**, 093302. (doi:10.1103/PhysRevFluids.2.093302)
67. Pollard J, Al-Izzi S, Morris RG. 2024 Gauge freedom and objective rates in the morphodynamics of fluid deformable surfaces: the Jaumann Rate vs. the material derivative. (http://arxiv.org/abs/2406.18014)
68. Nitschke I, Voigt A. 2024 Active nematodynamics on deformable surfaces. (http://arxiv.org/abs/2405.13683)
69. Jeffery GB. 1922 The motion of ellipsoidal particles immersed in a viscous fluid. *Proc. R. Soc. Lond. A* **102**, 161–179. (doi:10.1098/rspa.1922.0078)
70. Ericksen JL. 1991 Liquid crystals with variable degree of orientation. *Arch. Ration. Mech. Anal.* **113**, 97. (doi:10.1007/BF00380413)
71. De Gennes PG, Prost J. 1993 *The physics of liquid crystals*, vol. 83. Oxford, UK: Oxford University Press.
72. Virga EG. 2018 *Variational theories for liquid crystals*. Boca Raton, FL: CRC Press.
73. Leslie FM. 1968 Some constitutive equations for liquid crystals. *Arch. Ration. Mech. Anal.* **28**, 265–283. (doi:10.1007/BF00251810)
74. Frank FC. 1958 I. Liquid crystals. On the theory of liquid crystals. *Discuss. Faraday Soc.* **25**, 19–28. (doi:10.1039/df9582500019)
75. Canevari G, Segatti A. 2018 Defects in nematic shells: a Γ-convergence discrete-to-continuum approach. *Arch. Ration. Mech. Anal.* **229**, 125–186. (doi:10.1007/s00205-017-1215-z)
76. Pearce D. 2020 Defect order in active nematics on a curved surface. *New J. Phys.* **22**, 063051. (doi:10.1088/1367-2630/ab91fd)
77. Napoli G, Turzi S. 2020 Spontaneous helical flows in active nematics lying on a cylindrical surface. *Phys. Rev. E* **101**, 022701. (doi:10.1103/PhysRevE.101.022701)
78. Nestler M, Nitschke I, Löwen H, Voigt A. 2020 Properties of surface Landau–de Gennes Q-tensor models. *Soft Matter* **16**, 4032–4042. (doi:10.1039/C9SM02475A)
79. Bretherton FP. 1962 The motion of rigid particles in a shear flow at low Reynolds number. *J. Fluid Mech.* **14**, 284–304. (doi:10.1017/S002211206200124X)
80. Thijssen K. 2020 Active nematics with anisotropic friction: the decisive role of the flow aligning parameter. *Soft Matter* **16**, 2065. (doi:10.1039/C9SM01963D)
81. Hundsdorfer W, Verwer J. 2003 *Numerical solution of time-dependent advection-diffusion-reaction equations*. Berlin, Heidelberg: Springer.
82. Quarteroni A, Valli A. 2008 *Numerical approximation of partial differential equations*. Berlin Heiderberg, Germany: Springer Verlag.
83. Turner AM, Vitelli V, Nelson DR. 2010 Vortices on curved surfaces. *Rev. Mod. Phys.* **82**, 1301–1348. (doi:10.1103/RevModPhys.82.1301)
84. Giomi L, Bowick MJ, Mishra P, Sknepnek R, Cristina Marchetti M. 2014 Defect dynamics in active nematics. *Phil. Trans. R. Soc. A* **372**, 20130365. (doi:10.1098/rsta.2013.0365)
85. Thampi S, Yeomans J. 2016 Active turbulence in active nematics. *Eur. Phys. J. Spec. Top.* **225**, 651–662. (doi:10.1140/epjst/e2015-50324-3)
86. Zhu C, Lee C, Rangamani P. 2022 Mem3DG: modeling membrane mechanochemical dynamics in 3D using discrete differential geometry. *Biophys. Rep.* **2**, 100062. (doi:10.1016/j.bpr.2022.100062)
87. Zhu C, Saintillan D, Chern A. 2024 Stokes flow of an evolving fluid film with arbitrary shape and topology. *J. Fluid Mech.* **1003**, R1. (doi:10.1017/jfm.2024.1208)
88. Nitschke I, Voigt A. 2023 Beris-Edwards models on evolving surfaces: a Lagrange-d'alembert approach. (http://arxiv.org/abs/2311.06240)
89. Metselaar L, Yeomans JM, Doostmohammadi A. 2019 Topology and morphology of self-deforming active shells. *Phys. Rev. Lett.* **123**, 208001. (doi:10.1103/PhysRevLett.123.208001)
90. Zhu C. 2025 CunchengZhu/Riemannian-active-nematics-2024: Publication. *Zenodo*. (doi:10.5281/zenodo.14828306)
91. Zhu C, Saintillan D, Chern A. 2025 Supplementary material from: Active nematic fluids on Riemannian two-manifolds. Figshare. (doi:10.6084/m9.figshare.c.7719737)